Chem Soc Rev

REVIEW ARTICLE

View Article Online
View Journal | View Issue

Cite this: *Chem. Soc. Rev.*, 2023, **52**, 7170

π-Electronic ion pairs: building blocks for supramolecular nanoarchitectonics *via* $^{i}\pi$–$^{i}\pi$ interactions

Yohei Haketa, † Kazuhisa Yamasumi† and Hiromitsu Maeda *

The pairing of charged π-electronic systems and their ordered arrangement have been achieved by $^{i}\pi$–$^{i}\pi$ interactions that are derived from synergetically worked electrostatic and dispersion forces. Charged π-electronic systems that provide ion pairs as building blocks for assemblies have been prepared by diverse strategies for introducing charge in the core π-electronic systems. One method to prepare charged π-electronic systems is the use of covalent bonding that makes π-electronic ions and valence-mismatched metal complexes as well as protonated and deprotonated states. Noncovalent ion complexation is another method used to create π-electronic ions, particularly for anion binding, producing negatively charged π-electronic systems. Charged π-electronic systems afford various ion pairs, consisting of both cationic and anionic π-systems, depending on their combinations. Geometries and electronic states of the constituents in π-electronic ion pairs affect the photophysical properties and assembling modes. Recent progress in π-electronic ion pairs has revealed intriguing characteristics, including the transformation into radical pairs through electron transfer and the magnetic properties influenced by the countercations. Furthermore, the assembly states exhibit diversity as observed in crystals and soft materials including liquid-crystal mesophases. While the chemistry of ion pairs (salts) is well-established, the field of π-electronic ion pairs is relatively new; however, it holds great promise for future applications in novel materials and devices.

Received 24th July 2023

DOI: 10.1039/d3cs00581j

rsc.li/chem-soc-rev

Department of Applied Chemistry, College of Life Sciences, Ritsumeikan University, Kusatsu 525-8577, Japan. E-mail: maedahir@ph.ritsumei.ac.jp
† These authors equally contributed to this work.

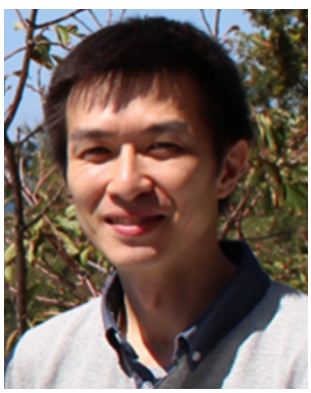

Yohei Haketa

Yohei Haketa received his PhD degree in 2011 from Ritsumeikan University, under the guidance of Prof. Hiromitsu Maeda, focusing on the assemblies of π-conjugated anion receptors. He was selected as a Research Fellow of the Japan Society for the Promotion of Science (JSPS) in 2009–2012. After working in Asahi Kasei Corporation as a researcher (2012–2015), he joined the group of Prof. Hiromitsu Maeda at Ritsumeikan University as a postdoctoral fellow in 2015 and started an academic career as an assistant professor in 2017, and, in 2019, he became a lecturer.

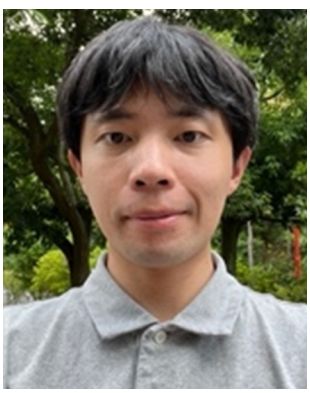

Kazuhisa Yamasumi

Kazuhisa Yamasumi received his PhD degree in 2020 from Kyushu University under the guidance of Prof. Hiroyuki Furuta, focusing on isomeric porphyrin analogues. His PhD research was focused on the synthesis of infrared dyes based on the expanded or π-extended isomeric porphyrin analogues. He joined the group of Prof. Hiromitsu Maeda at Ritsumeikan University as a postdoctoral fellow in 2020. His current research focuses on π-electronic ion-pairing assemblies.

1. Introduction

Various functional materials that are applied in organic electronics can be fabricated by π-electronic systems that have electronic states depending on their core structures and substituents.[1] Electronic properties of such materials are modulated by the arrangement of constituents *via* noncovalent interactions.[2] Understanding and utilization of these interactions offer valuable insights for designing captivating assembled structures and materials. Noncovalent interactions, such as π–π, hydrogen-bonding and van der Waals interactions, are facilitated by combining fundamental intermolecular forces, including (i) electrostatic, induction and dispersion forces as long-range forces originating from coulombic forces and (ii) exchange-repulsion and charge-transfer (CT) forces as short-range forces caused by interorbital interaction.[3] Electronically neutral π-electronic systems form stacking assemblies by dispersion forces, the main components of π–π interactions.

The introduction of charge into π-electronic systems drastically changes the assembling behaviour based on electrostatic forces. Electrostatic and dispersion forces play a significant role in the arrangement of charged π-electronic systems in their assemblies.[4,5] The assemblies feature stacking structures, with the fundamental units being π-stacked ion pairs (*π-sips*). These *π-sips* represent characteristic forms of paired oppositely charged π-electronic systems (π-electronic ion pairs) (Fig. 1a).[6] *π-Sips* form various ion-pairing assemblies with the modes of charge-by-charge assemblies, wherein oppositely charged species are alternately stacked; moreover, they provide charge-segregated assemblies, in which identically charged species are stacked *via* dissociation and recombination (Fig. 1a). The assembling modes are modulated by the geometries and electronic states of charged π-electronic systems in ion pairs. Various π-electronic ion pairs can be formed by combining π-electronic cations and anions; ten kinds of cations and ten kinds of anions ideally afford 100 kinds of ion pairs. Chemistry of π-electronic ion-pairing assemblies started in 2010 with the fabrication of charge-by-charge assemblies comprising π-electronic receptor–anion complexes and π-electronic cations in the form of single crystals, supramolecular gel and liquid crystals (*vide infra*, Section 3.1).[7,8] In 2021, cooperative interactions involving electrostatic and dispersion forces were proposed as $^{i}\pi$–$^{i}\pi$ interactions *via* detailed experimental and theoretical investigations, including single-crystal X-ray analysis and energy decomposition analysis (EDA) for solid-state ion-pairing assemblies.[9] As previously defined, the $^{i}\pi$ in "$^{i}\pi$–$^{i}\pi$ interactions" represents π-electronic ions and charged π-electronic systems. $^{i}\pi$–$^{i}\pi$ Interactions induce stacking of oppositely charged

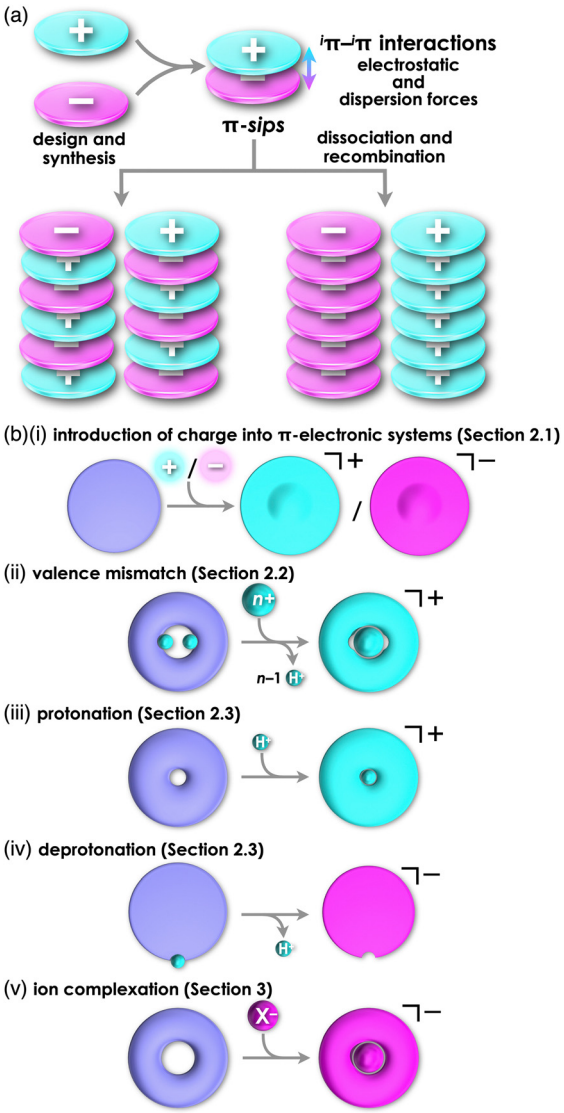

Fig. 1 (a) Conceptual diagrams for the formation of *π-sips* (top) and charge-by-charge (bottom left) and charge-segregated assemblies (bottom right) comprising charged π-electronic species and (b) formation of charged π-electronic systems *via* "covalent approaches" by (i) introducing charges directly into the core, (ii) valence mismatch by metal complexation, denoted by cation formation as a representative and (iii) protonation and (iv) deprotonation at the basic and acidic sites, respectively, along with (v) ion complexation, as "noncovalent approach" in contrast to (i–iv), denoted by anion binding as a representative.

Hiromitsu Maeda

Hiromitsu Maeda received his PhD degree in 2004 from Kyoto University, under the guidance of Prof. Hiroyuki Furuta (Kyushu University) and Prof. Atsuhiro Osuka, after spending three months in the Sessler group, the University of Texas at Austin, in 2001. In 2004, he started an academic career in Department of Bioscience and Biotechnology, Faculty of Science and Engineering, Ritsumeikan University. In 2008, he was transferred to College of Pharmaceutical Sciences, wherein he was promoted to a professor in 2014. In 2016, he moved to Department of Applied Chemistry, College of Life Sciences. He has been awarded several prizes, including ChemComm Emerging Investigator Lectureship (2012) and Fellow of the RSC (2015).

π-electronic systems owing to the enhanced contribution of attractive electrostatic and dispersion forces, resulting in the formation of *π-sips* and their assemblies. For identically charged π-electronic systems, $^{i}\pi$–$^{i}\pi$ interactions can be modulated depending on the balance of electrostatic and dispersion forces, facilitating the formation of charge-segregated assemblies. The electronic states of charged π-electronic systems are closely related with their HOMO (highest occupied molecular orbital) and LUMO (lowest unoccupied molecular orbital), which are essential in redox processes, photophysical properties and reactivity. Stacked states of oppositely charged π-electronic systems with relatively high HOMO levels for anions and low LUMO levels for cations can induce charge- and electron-transfer behaviours. Diverse charged π-electronic systems have been reported as potential components of π-electronic ion pairs, including commercially available reagents. This review article summarizes the ion pairs comprising π-electronic cations and anions and their properties for potential applications as functional materials.

Charged π-electronic systems as the components of π-electronic ion pairs can be obtained by diverse methods. A charge can be introduced by covalent and noncovalent approaches (Fig. 1b). In Section 2, several strategies using "covalent approaches" for the preparation of π-electronic charged species are displayed, such as the use of aromaticity and valence mismatch (Fig. 1b(i,ii)). Protonated and deprotonated species of π-electronic systems, using the coordination bond between a proton and a basic site for the former, are also included (Fig. 1b(iii,iv)). Section 3 demonstrates the formation of pseudo-π-electronic ions through the complexation of π-electronic systems and inorganic ions by noncovalent interactions (Fig. 1b(v)). This process results in the creation of ion pairs and their assemblies, including the charged π-electronic systems discussed in Section 2. Although various pseudo-π-electronic cations and anions are formed using this method, anion-complexation strategies are the main focus. In Section 4, pairs of the charged π-electronic systems shown in Section 2 are summarized as solution-state *π-sips* and assemblies in crystalline states and mesophases. The photophysical properties of π-electronic ion pairs are also displayed. However, radical ions derived from electronically neutral closed-shell π-systems are not included in this review.

2. π-Electronic systems with charge introduced by covalent approaches: components of ion pairs with non-π-electronic counterions

Diverse strategies, classified as covalent approaches, are available for the production of charged π-electronic systems (Fig. 1b(i–iv)). The introduced charge in π-electronic systems can be delocalized for stabilization. Aromaticity achieved by charge introduction further contributes to the stabilization of charged species. Valence mismatch between π-electronic ligands and metal ions also provides charged π-electronic systems. Furthermore, protonation and deprotonation of electronically neutral π-electronic systems are facile approaches to forming positively and negatively charged π-electronic systems.

2.1. Introduction of charge into π-electronic systems

Carbocations and carbanions are generally less stable species, whose reactivity can be reduced by delocalizing the charges through extended π-systems (Fig. 1b(i)). For example, the triphenylmethyl cation (tritylium) $\mathbf{1}^+$ (Fig. 2a(i)), which can be used as a Lewis acid in various organic synthesis, is more stable than the *tert*-butyl cation.[10] The stability of cations is further improved by introducing electron-donating groups, as seen in crystal violet ($\mathbf{2}^+$ as a cation part, Fig. 2a(ii)).[11] Moreover, the π-extension of tritylium can be achieved by reducing the steric repulsion between the *ortho*-CH units to form planar structures. Bridging two aryl groups with an atom results in the formation of planar structures as observed in rhodamine B ($\mathbf{3a}^+$ as a cation part, Fig. 2b(i)), which possesses a planar tricyclic π-unit that is characteristic of xanthene dyes.[12,13] Rhodamine B, represented as $\mathbf{3a}^+$-Cl^-, exhibits strong absorption and fluorescence bands in the visible region at 554 and 627 nm, respectively, in MeOH. These properties make the dye suitable for fluorescence imaging applications.[13a] Furthermore, replacement of the oxygen with other heteroatoms, like phosphorus in $\mathbf{3b}^+$ (Fig. 2b(ii)), alters the electronic states and photophysical properties. The absorption and emission maxima of $\mathbf{3b}^+$ in a phosphate-buffered saline (PBS) buffer (pH = 7.4) are observed at 712 and 740 nm, respectively.[13c] Notably, various positively charged dyes, as seen in tritylium, crystal violet and rhodamine B, are commercially available.

Bridging the *ortho*-CH units of the three aryl groups of tritylium with three N or O linkers affords planar trianguleniums such as triazatriangulenium ($TATA^+$)[14] (Fig. 3a) and trioxatriangulenium ($TOTA^+$)[15] $\mathbf{4a}^+$ (Fig. 3b(i)). A variety of triangulenium derivatives, including less planar helicene structures,[14a] have been reported thus far for the use in various applications such as phase transition catalysis, bioimaging and DNA intercalation. In particular, the planar charged π-electronic systems are suitable for efficient electron-accepting properties and stacking in various supramolecular assemblies.[16] For example, $TATA^+$ bearing ether

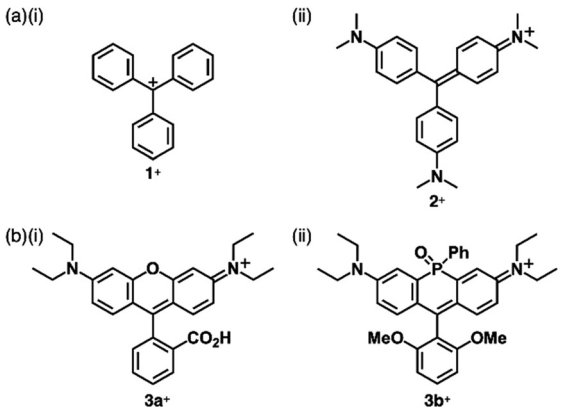

Fig. 2 Representative charged triarylmethane dyes (a) $\mathbf{1}^+$ and $\mathbf{2}^+$ and (b) $\mathbf{3a,b}^+$.

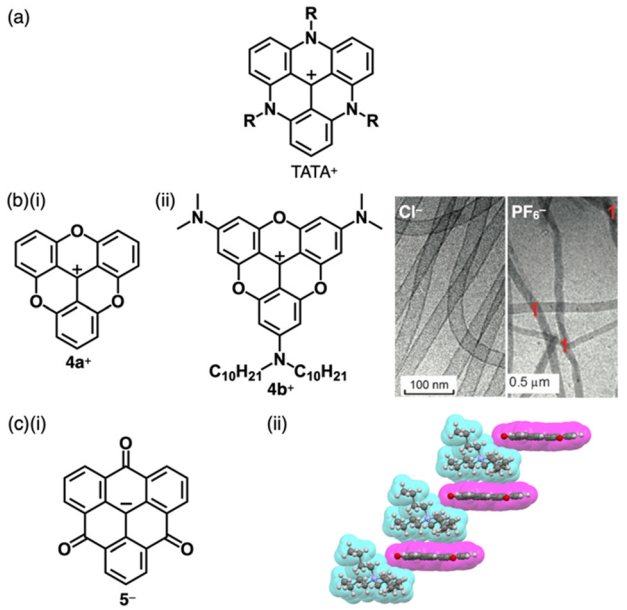

Fig. 3 (a) General structure of TATA$^+$, (b) (i) TOTA$^+$ **4a**$^+$ and (ii) alkyl-substituted TOTA$^+$ **4b**$^+$ and cryo-TEM images of nanostructures of **4a**$^+$-X$^-$ (X$^-$ = Cl$^-$ (left) and PF_6^- (right)) formed in water (10 vol% CH_3CN) (redrawn from ref. 15c. Copyright 2014 Wiley) and (c) (i) trioxotriangulene anion **5**$^-$ and (ii) single-crystal X-ray structure of TBA$^+$-**5**$^-$ (redrawn from a cif file: 1303470). Atom colour code in (c) and the following figures: grey, white, blue and red in the ball-and-stick models refer to carbon, hydrogen, nitrogen and oxygen, respectively, whereas cyan and magenta in the space-filling models refer to cation and anion, respectively.

chains with a terminal hydroxy unit has been used as a visible-light absorbing photosensitizer in metal-catalyzed hydrogen production in water.[16a] Conversely, TOTA$^+$ with aliphatic alkyl chains at one terminal (**4b**$^+$, Fig. 3b(ii)) formed counteranion-depending nanoscale assemblies comprising stacked **4b**$^+$ (Fig. 3b(ii)).[15c] Planarization can also be applied to anion species: bridging triarylmethyl anion with three electron-withdrawing carbonyl groups afforded the trioxotriangulene anion **5**$^-$ (Fig. 3c(i)).[17] **5**$^-$ is thermodynamically stabilized owing to the charge-delocalized closed-shell structure, forming the ion pair with tetrabutylammonium (TBA$^+$). Single-crystal X-ray analysis of TBA$^+$-**5**$^-$ revealed that TBA$^+$ and planar **5**$^-$ were alternately stacked to form a columnar structure (Fig. 3c(ii)).

Allyl ions and their extended ionic polymethines are stabilized by introducing two aryl groups at both ends (Fig. 4a).[18] Various derivatives were synthesized as polymethine dyes with terminal aryl groups such as pyrylium, quinolinium[18e] (**6a**–**c**$^+$, Fig. 4b(i)) and benzothiazolium[18b] (**7a**–**c**$^+$, Fig. 4b(ii)). As polymethine dyes exhibit sharp absorption bands in the visible-to-near infrared (NIR) region depending on the length of the polymethine chains and the terminal π-electronic systems, cationic dyes are applied as fluorescent probes, laser dyes and photovoltaic materials. Generally, the polymethine dyes exhibit red-shifted absorption bands depending on the length of the linker polymethine units, as seen in the absorption maxima of 425, 558 and 660 nm for **7a**–**c**$^+$, respectively. The photophysical properties are affected by aggregation due to the significant

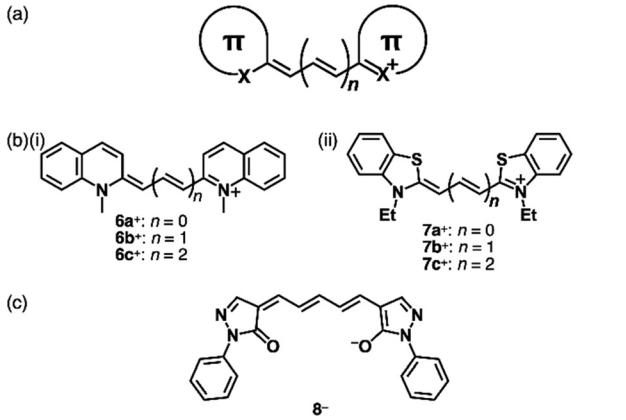

Fig. 4 (a) General structure of polymethine dyes, (b) positively charged polymethine dyes based on (i) *N*-methylquinolium (**6a**–**c**$^+$) (ii) benzothiazolium (**7a**–**c**$^+$) and (c) negatively charged polymethine dye based on deprotonated oxonol (**8**$^-$).

exciton coupling caused by the large transition dipole moments. Therefore, assemblies of polymethine dyes have attracted great attention to date.[18a,19] Furthermore, negatively charged π-electronic systems (*e.g.*, **8**$^-$, Fig. 4c) are stabilized by the introduction of electron-withdrawing terminal π-units, although applications are limited owing to decreased stability.[20]

Modifications at the centre of the polymethine chains affect the rigidity and modulate the photophysical properties.[18] The positive charge can be compensated by the introduction of negatively charged substituents at the polymethine chains, as seen in zwitterionic squarylium **9** (Fig. 5a) and croconium dyes.[21] These dyes are converted to the corresponding cations by introducing alkyl groups at the anionic site as seen in **10**$^+$ (Fig. 5a).[22] In the crystal structures of ion pairs **10**$^+$-X$^-$ (X$^-$ = OTf$^-$ and $B(C_6F_5)_4^-$), the **10**$^+$ units are stacked by themselves.

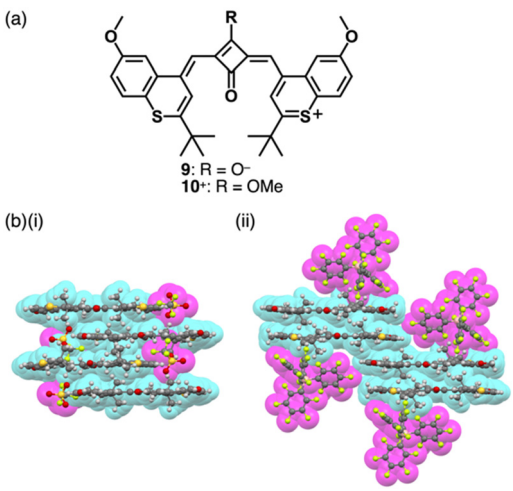

Fig. 5 (a) Zwitterionic squarylium dye **9** and cationic squarylium dye **10**$^+$ and (b) single-crystal X-ray structures of (i) **10**$^+$-OTf$^-$ and (ii) **10**$^+$-$B(C_6F_5)_4^-$ (redrawn from cif files: 2214017 and 2214019). Atom colour code in (b) and the following figures: pink, yellow green and dark yellow in the ball-and-stick models refer to boron, fluorine and sulfur, respectively.

Notably, the stacked $\mathbf{10}^+$ units exhibit antiparallel orientation to cancel their dipoles (Fig. 5b).[23] Furthermore, $\mathbf{10}^+$ shows sharp absorption bands in the NIR region, which are shifted depending on the assembling conditions (*vide infra*, Section 4.1).

Charged units can be stabilized by aromaticity.[24] A smallest class of aromatic compounds is cyclopropenium, a positively charged 2π electronic system (Fig. 6a(i)),[25] which is highly reactive and participates in various reactions. The stability of cyclopropenium is increased by the introduction of electron-donating units, as seen in $\mathbf{11}^+$ (Fig. 6a(ii)). Cycloheptatrienyl cation, tropylium (Tr^+), a 6π electronic system, is a relatively stable π-electronic cation (Fig. 6b).[26] In contrast, cyclopentadienide (Cp^-) as a negatively charged 6π electronic system is stable enough for various metallocenes (Fig. 6c(i)).[27] Delocalization of negative charges by π-extension can stabilize anions as seen in the tris(7*H*-dibenzo[*c*,*g*]fluorenylidenemethyl)methyl anion (Kuhn's anion) $\mathbf{12}^-$ (Fig. 6c(ii)), a genuine hydrocarbon charged π-electronic anion including Cp^- units.[28] Kuhn's anion has been synthesized as ion pairs with various cations, including π-electronic cations. Owing to the anion's easily oxidizable nature, the ion pairs must be handled under an inert atmosphere and light shading conditions to prevent unwanted reactions or degradation.

The stability of Cp^- can be enhanced by the introduction of electron-withdrawing units. For example, various ion pairs have incorporated pentamethoxycarbonylcyclopentadienide $\mathbf{13}^-$ (Fig. 7a(i)).[29] The crystal structure of TMA$^+$-$\mathbf{13}^-$ (TMA$^+$ = tetramethylammonium) revealed that dihedral angles between methoxycarbonyl CO_2C planes and the core cyclopentadienide unit were within a range of 15.7°–85.9°, exhibiting a nonplanar structure (Fig. 7a(ii)).[30] Replacement of the ester groups with cyano groups as less bulky electron-withdrawing groups allows the production of planar anions that are available for more effective stacking with charged π-electronic systems. Since the synthesis of pentacyanocyclopentadienide ($PCCp^-$)[31] by Webster in 1965 (Fig. 7b(i)),[31a] the anion has been used as the building block of solid-state coordination networks in combination with metal ions.[32] Exchange of the countercation with other cations *via* ion-pair metathesis as an ion-exchange protocol based on hard and soft acids and bases (HSAB) theory (details are summarized in Section 4) afforded various ion pairs, demonstrating unique assembled structures.[33,34] Single-crystal X-ray analysis of $(C_4H_9)(CH_3)_3N^+$-$PCCp^-$ exhibited a columnar structure comprising stacking of $PCCp^-$ with a distance of 3.42 Å (Fig. 7b(ii)). Notably, $(C_4H_9)(CH_3)_3N^+$ is located proximally to $PCCp^-$, constructing a charge-segregated assembly. Furthermore, a charge-segregated assembly in the form of a hexagonal columnar (Col_h) structure was observed in the liquid crystal mesophase of $(C_{12}H_{25})_3CH_3N^+$-$PCCp^-$ (Fig. 7b(iii)), and its hole mobility was estimated to be 0.4 $cm^2\ V^{-1}\ s^{-1}$ using field-induced time-resolved microwave conductivity (FI-TRMC) technique.[33]

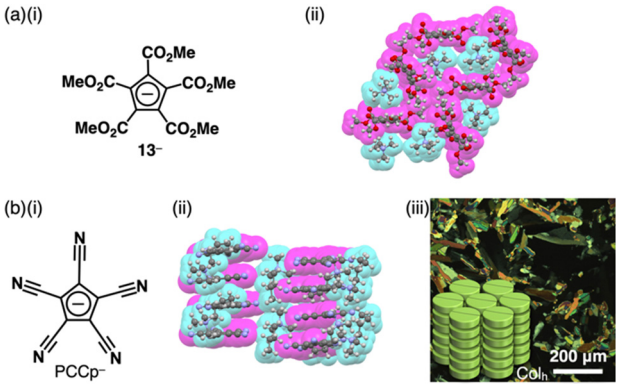

Fig. 7 (a) (i) Pentamethoxycarbonylcyclopentadienide $\mathbf{13}^-$ and (ii) single-crystal X-ray structure of TMA$^+$-$\mathbf{13}^-$ and (b) (i) pentacyanocyclopentadienide ($PCCp^-$), (ii) single-crystal X-ray structure of $(C_4H_9)(CH_3)_3N^+$-$PCCp^-$ and (iii) POM of liquid crystal mesophase of $(C_{12}H_{25})_3CH_3N^+$-$PCCp^-$ at 70 °C upon cooling (redrawn from ref. 33. Copyright 2016 Wiley). The crystal structures are redrawn from cif files: 1137646 and 1431736.

Replacement of carbons with heteroatoms in aromatic π-electronic systems affords charged aromatic π-electronic systems (Fig. 8). Notably, the replacement of a CH unit in benzene with substituted nitrogen and oxygen/sulfur produces pyridinium, pyrylium and thiopyrylium, respectively ($\mathbf{14a}$–$\mathbf{c}^+$ as triphenyl-substituted derivatives, Fig. 8a).[35] Taking advantage

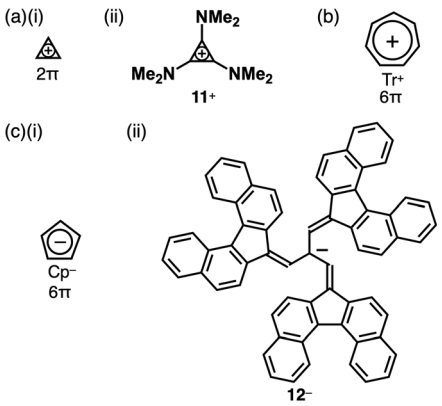

Fig. 6 Representative charged π-electronic systems stabilized by aromaticity: (a) (i) cyclopropenium and (ii) tris(dimethylamino)-substituted derivative $\mathbf{11}^+$, (b) tropylium and (c) (i) cyclopentadienide and (ii) Kuhn's anion $\mathbf{12}^-$.

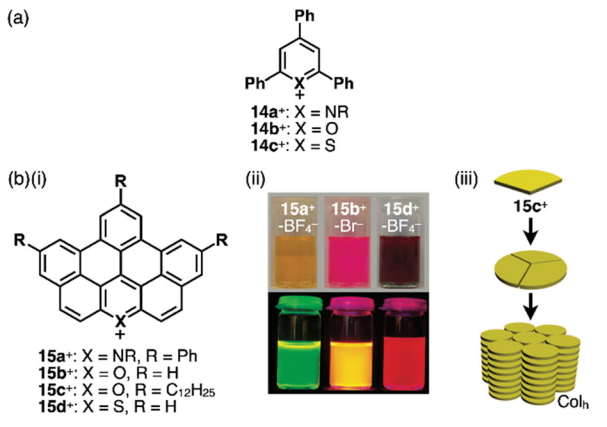

Fig. 8 (a) Triphenylpyridinium and triphenylpyryliums $\mathbf{14a}$–$\mathbf{c}^+$ and (b) (i) π-extended pyridinium and pyryliums $\mathbf{15a}$–$\mathbf{d}^+$, (ii) photographs of CH_2Cl_2 solutions of $\mathbf{15a}^+$-BF_4^-, $\mathbf{15b}^+$-Br^- and $\mathbf{15d}^+$-BF_4^- (top: under visible light, bottom: under UV) and (iii) packing diagram of $\mathbf{15c}^+$-Br^- (redrawn from ref. 36. Copyright 2009 ACS).

of the electron-deficient nature and moderate reactivity, 2,4,6-triarylpyryliums (*e.g.*, **14b**$^+$) are used as photocatalysts and building blocks of extended π-electronic systems.[35b] Some charged species, such as pyridinium, are stable under ambient conditions. Other charged π-electronic systems can be stabilized by π-extensions as seen in peripherally heteroatom-containing phenanthro[2,3,4,5-*pqrab*]perylenes as π-extended pyridinium, pyrylium and thiopyrylium **15a–d**$^+$ reported by Feng, Müllen and coworkers (Fig. 8b(i)),[36] whose electronic properties clearly depend on the introduced heteroatoms. Red-shifted UV/vis absorption and emission maxima occur at 512/531, 573/594 and 600/643 nm for **15a,b,d**$^+$ corresponding to BF_4^-, Br^- and BF_4^- ion pairs, respectively, in CH_2Cl_2 (Fig. 8b(ii)). Dodecyl-substituted **15c**$^+$ as a Br^- ion pair forms liquid crystal mesophases based on the Col_h structure (Fig. 8b(iii)). Conversely, the internal carbon of naphthalene can be replaced with nitrogen, resulting in quinolizinium as the smallest N-doped polycyclic aromatic hydrocarbon (PAH).[37] Electron-deficient planar charged π-electronic systems with appropriate sizes and substituents can be applied to DNA intercalation. Representative π-extended N-doped PAHs include 9-phenylbenzo[1,2]quinolizino[3,4,5,6-*fed*]-phenanthridinylium (PQP$^+$) cations **16a,b**$^+$ (Fig. 9a), synthesized from a 2,4,6-triphenylpyrylium salt.[38] PQP$^+$ forms charge-segregated assemblies *via* $^i\pi$–$^i\pi$ interactions.[38b] In particular, PQP$^+$ ion pairs **16b**$^+$-X$^-$ (X$^-$ = Cl$^-$ and BF_4^-) form counteranion-dependent ion-pairing assemblies with distinct morphologies (Fig. 9b).[38a] TEM images of the assemblies exhibit nanoribbons and nanotubes for the Cl$^-$ and BF_4^- ion pairs, respectively, suggesting that even small counteranions have important roles in the arrangement of charged π-electronic units and resulting organized structures.

Porphyrin, consisting of four pyrrole rings bridged by methine units, is an 18π electronic aromatic macrocycle.[39] Porphyrin and its analogues play important roles in biological systems such as metabolism and photosynthesis. The large π-electronic system of porphyrin contributes to charge delocalization and, thus, stabilization of charged species. Various stacking assemblies can be formed from porphyrin derivatives.[19,40] Therefore, porphyrin is an excellent building block for charged π-electronic systems as components of π-electronic ion-pairing assemblies. In addition, the redox properties of porphyrin can be modulated by peripheral substituents. The introduction of substituted N and O/S at one of the porphyrin *meso* positions affords positively charged heteroatom-containing porphyrins **17a–c**$^+$ (Fig. 10a(i)).[41] The

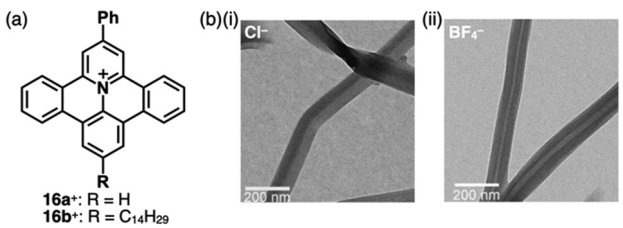

Fig. 9 (a) PQP$^+$ **16a,b**$^+$ and (b) TEM images of aggregates in MeOH (1 mM): (i) **16b**$^+$-Cl$^-$ and (ii) **16b**$^+$-BF_4^- (redrawn from ref. 38a. Copyright 2007 Wiley).

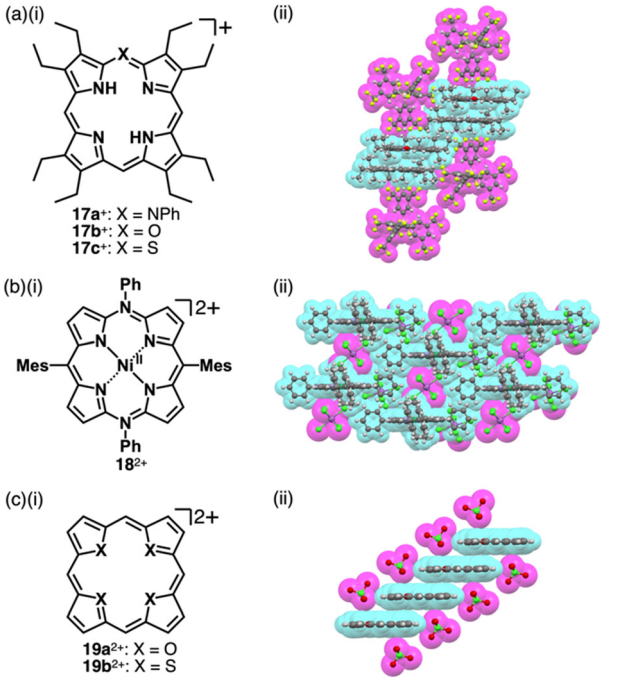

Fig. 10 (a) (i) Heteroatom-containing porphyrins **17a–c**$^+$ and (ii) single-crystal X-ray structure of **17a**$^+$-BAr^{F-}, (b) (i) tetraaryl-5,15-diazaporphyrin Ni^{II} complex **18**$^{2+}$ and (ii) single-crystal X-ray structure of **18**$^{2+}$-2$SbCl_6^-$ and (c) (i) core-modified porphyrins **19a,b**$^{2+}$ and (ii) single-crystal X-ray structure of **19a**$^{2+}$-2ClO_4^-. The crystal structures are redrawn from cif files: 2033992, 1437728 and 1166405. Atom colour codes in (b) (c) (ii) and the following figures: green, blue-green and purple in the ball-and-stick models refer to chlorine, nickel and antimony, respectively.

inner NH protons of **17a,c**$^+$ are located at the nitrogens in the *trans* positions, whereas those of **17b**$^+$ are located at those in the *cis* positions, far from the introduced *meso*-oxygen.[41b–d] This arrangement suggests charge delocalization and resulting polarized structures attributed to the introduced atoms. In the crystal structures of **17a–c**$^+$-BAr^{F-} (BAr^{F-} = $B(3,5\text{-}(CF_3)_2C_6H_3)_4^-$), the cations are stacked by themselves on the π-plane, while further stacking is inhibited by BAr^{F-} located on the π-plane (Fig. 10a(ii)). Furthermore, tetraaryl-5,15-diazaporphyrin Ni^{II} complex **18**$^{2+}$ as a dication in PF_6^- and $SbCl_6^-$ ion pairs can be obtained by oxidizing the corresponding neutral form with $AgPF_6$ or magic blue (Fig. 10b).[42] Moreover, a similar approach to the one mentioned in the previous paragraph can be applied to heterocyclic systems, where heteroatoms are converted to other heteroatoms with different valences. Heteroporphyrins **19a,b**$^{2+}$, whose inner nitrogens are replaced with chalcogens, form various charged π-electronic systems (Fig. 10c(i)).[43] In the crystal structure of the ClO_4^- ion pair, **19a**$^{2+}$ appears highly planar and forms a columnar structure, slip-stacking by itself on both sides (Fig. 10c(ii)). However, the thiophene units in **19b**$^{2+}$ are inclined by 22.8° and 3.7° in the crystal structure.[43c]

2.2. Charged π-electronic systems derived from valence mismatch

Charges in complexes comprising multiple units can be controlled by the valences of the components. Therefore, if the number of positive charges of metal ions is not matched with

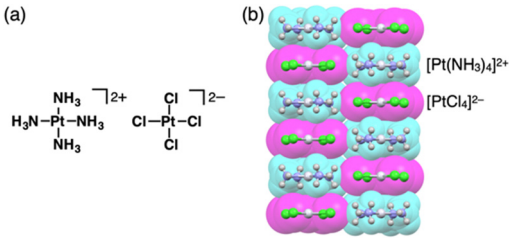

Fig. 11 Magnus' green salt: (a) ion-pairing form and (b) single-crystal X-ray structure (redrawn from a cif file: 2009952). Atom colour code in (b) and the following figures: light grey in the ball-and-stick models refers to platinum.

that of the total negative charges of ligands, the resulting complexes behave as charged species (Fig. 1b(ii)). Metal complexes with such a valence mismatch are used in Magnus' green salt: a salt comprising $[Pt(NH_3)_4]^{2+}$ and $[PtCl_4]^{2-}$, alternately arranged to form an anisotropic quasi 1D linear array in the solid state (Fig. 11).[44,45] The 1D structure of the aligned Pt^{II} complexes in Magnus' green salt is mainly constructed by the electrostatic force between the positively and negatively charged planar Pt^{II} complexes. The fascinating ion-pairing structure has stimulated numerous studies regarding the use of 1D arrays as electrically conductive wires. Importantly, the correlation between the geometries of the constituents and the assembled structure has been clearly demonstrated. This observation has prompted us to design and synthesize charged π-electronic species for fabricating various functional ion-pairing assemblies through $^{i}\pi$–$^{i}\pi$ interactions.

As π-electronic ligands in preparation for charged π-electronic species by valence mismatch, porphyrins serve as dianionic ligands owing to the two inner NH groups. Therefore, complexation with trivalent metal ions provides π-electronic cations accompanied by an anion for charge compensation. Versatile porphyrin complexes with trivalent metal ions such as Cr^{III}, Mn^{III}, Fe^{III} and Co^{III} have been prepared thus far.[39] Most of the metal complexes have axial ligands, which compensate for the positive charge and hamper the stacking of the resulting π-electronic systems. **20**$^+$, a porphyrin Fe^{III} complex with bulky triisopropylsilyloxy substituents, can be obtained in the neutral form coordinated by a Cl^- ligand.[46] Here, the Cl^- is exchanged with other anions by ion-pair metathesis with Ag^+ salts of weakly coordinating anions (ClO_4^-, OTf^- and SbF_6^-) (Fig. 12a). Hexabromocarborane anion ($CH_6B_{11}Br_6^-$)[47] is too bulky to approach the axial coordination site owing to the steric hindrance, resulting in π-electronic cations without axial ligands. Boron complexes of subporphyrins usually exhibit bowl-like structures attributed to the structural distortion caused by axial coordination at the boron centre.[48] Treatment of methoxide-coordinated subporphyrin boron complex with $Et_3Si[CH_6B_{11}Br_6]$ afforded a planar subporphyrin cation **21**$^+$ as an ion pair with $CH_6B_{11}Br_6^-$ (Fig. 12b).[49] Conversely, porphyrin Au^{III} complexes, whose metal centre is in a d^8 electronic state, generally have no axial ligands (*e.g.*, **22a**–**e**$^+$, Fig. 13a).[6,50–53] Thus, porphyrin Au^{III} complexes readily form ion pairs in combination with desired anions and can be adopted as building blocks for π-electronic ion-pairing assemblies.[6,52]

Porphyrins can be complexed with Au^{III} using different procedures. One well-known method involves using $KAuCl_4$ in refluxing AcOH.[51a] Other synthetic approaches, such as the uses of $HAuCl_4{\cdot}4H_2O$/AgOTf/NaOAc[51d] and $Au(tht)_2BF_4$ (tht = tetrahydrothiophene)/2,6-lutidine,[51c] can be applied depending on the reactivity of the porphyrins. Counteranions of the porphyrin Au^{III} complexes after the Au^{III} complexation are mainly derived from the corresponding Au^{III} reagents. To exchange the counteranions to Cl^-, porphyrin Au^{III} complex ion pairs can be passed through an ion-exchange resin (Amberlite). Moreover, the Cl^- ions can be exchanged with inorganic salts containing the desired anions through ion-pair metathesis, resulting in various ion pairs.

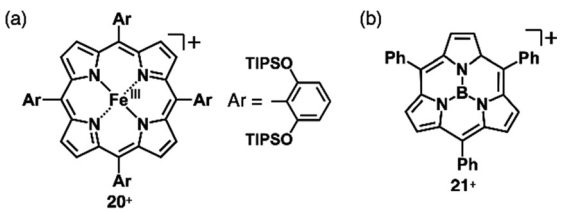

Fig. 12 Positively charged porphyrin and analogue formed by valence mismatch: (a) porphyrin Fe^{III} complex **20**$^+$ and (b) subporphyrin boron complex **21**$^+$.

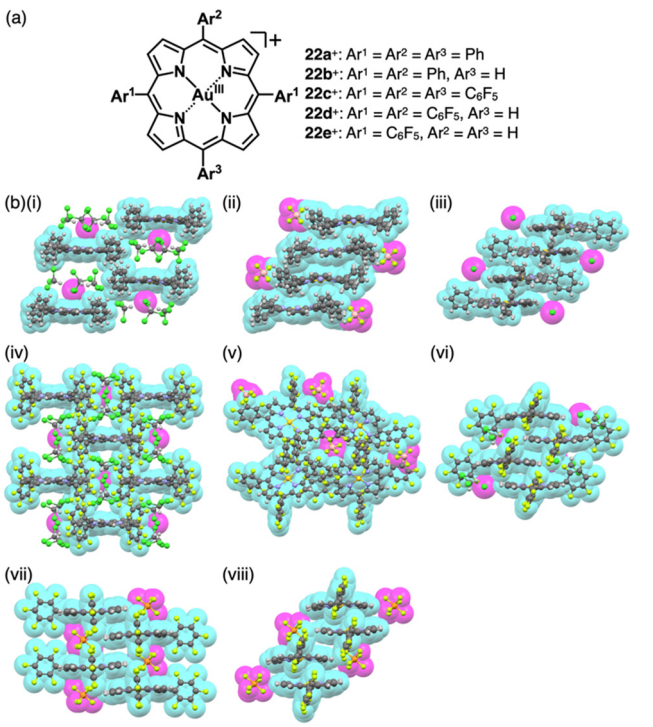

Fig. 13 Positively charged porphyrins formed by valence mismatch: (a) *meso*-arylporphyrin Au^{III} complexes **22a**–**e**$^+$ and (b) single-crystal X-ray structures of (i) **22a**$^+$-Cl^-, (ii) **22a**$^+$-BF_4^-, (iii) **22b**$^+$-Cl^-, (iv) **22c**$^+$-Cl^-, (v) **22c**$^+$-BF_4^-, (vi) **22d**$^+$-Cl^-, (vii) **22d**$^+$-PF_6^- and (viii) **22e**$^+$-PF_6^- (redrawn from cif files: 1877987, 1877988, 2226630, 1904175, 1904176, 1904174, 1904178 and 1904177). Atom colour codes in (b) and the following figures: orange and yellow in the ball-and-stick models refer to phosphorus and gold, respectively.

The high stability of these ion pairs allows for purification using silica gel column chromatography.[52]

Single-crystal X-ray analysis revealed the exact structures of porphyrin Au^{III} complexes with no axial ligands. **22a**$^+$-Cl^- in a pseudo-polymorph shows a columnar structure based on a charge-by-charge assembly including Cl^- with four co-crystallized $CHCl_3$ molecules (Fig. 13b(i)).[51b,52a] The proximal Au···Cl^- distance was 3.12 Å, comparable to the sum of the ionic radii of Au^{3+} and Cl^-, suggesting the formation of a contact ion pair. In addition, the line passing through both Au and Cl has an angle of 80.2° to the mean plane of **22a**$^+$. The non-90° angle indicates that Cl^- is not directly coordinated to the core Au^{III} in proximity to **22a**$^+$. Instead, it exists as a π-electronic cation, and the interaction is primarily based on electrostatic interactions. In contrast to the charge-by-charge structure of **22a**$^+$-Cl^-, charge-segregated assemblies are formed in **22a**$^+$-BF_4^- and **22a**$^+$-PF_6^- (Fig. 13b(ii)), exhibiting columnar structures of stacked **22a**$^+$ with stacking distances of 3.73/3.88 and 3.87/3.89 Å, respectively.[52a] Conversely, ion pairs of *meso*-triphenyl-substituted **22b**$^+$ with Cl^- form charge-segregated assemblies with stacking distances of 3.50 and 3.74 Å (Fig. 13b(iii)), whereas **22b**$^+$-PF_6^- exhibits a stacked dimer of **22b**$^+$ with a stacking distance of 3.46 Å. In both cases, counteranions are located at either side of **22b**$^+$.[52b]

The assembling behaviours of the ion pairs are affected by the introduction of electron-withdrawing C_6F_5 groups (**22c–e**$^+$, Fig. 13a).[52b] The Cl^- in **22c**$^+$-Cl^- is in contact with the β-CH units of two porphyrins, resulting in layered structures separated by the bulky C_6F_5 groups (Fig. 13b(iv)). Therefore, the Au···Cl distance (7.08 Å) is much longer than those of **22a**$^+$-Cl^- (3.00 and 3.12 Å). Meanwhile, in **22c**$^+$-BF_4^-, the C_6F_5 groups are arranged around BF_4^- with interionic π···F short contacts (Fig. 13b(v)). In **22d**$^+$-Cl^-, Cl^- is separated from the Au^{III} centre by CH_2Cl_2 (Fig. 13b(vi)) and is located proximally to the *meso*-CH of **22d**$^+$. The arrangements of the cations and PF_6^- in **22d**$^+$-PF_6^- and **22e**$^+$-PF_6^- are similar to that of **22d**$^+$-Cl^-, although the interplanar distances are slightly longer (3.50–3.84 Å) than that of **22d**$^+$-Cl^- (Fig. 13b(vii,viii)).[52b]

A similar approach can be applied to divalent metal complexes with monoanionic ligands such as thiaporphyrins (tetraphenylthiaporphyrin Ni^{II} complex **23**$^+$ as a representative structure, Fig. 14a).[39,54] In 1989, Latos-Grażyński, Balch and coworkers reported **23**$^+$ and Cu^{II} and Fe^{II} complexes as Cl^- ion pairs.[54] In the crystal structure of **23**$^+$-Cl^-, the Ni···Cl^- distance is 2.28 Å, indicating the axial coordination. The thiophene unit of **23**$^+$ is inclined by ~25°, leading to a less planar structure. Furthermore, ion pair **23**$^+$-PF_6^-, prepared by ion-pair metathesis of **23**$^+$-Cl^- with $AgPF_6$, forms the solid-state stacked dimer structure, wherein the S···N distance is 3.77 Å owing to chalcogen bonding (Fig. 14b).[55]

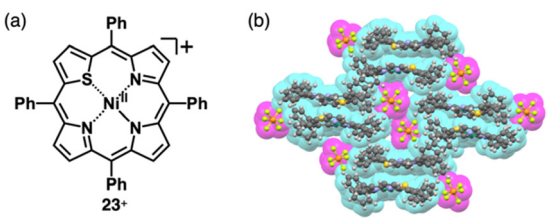

Fig. 14 (a) Thiaporphyrin Ni^{II} complex **23**$^+$ and (b) single-crystal X-ray structure of **23**$^+$-PF_6^- (redrawn from a cif file: 2167302).

Similarly, anionic species can be obtained by complexing divalent metals with trianionic ligands such as corrole. The introduction of electron-withdrawing substituents at appropriate positions is required for stable π-electronic anions. Gross *et al.* reported *meso*-C_6F_5-substiuted corrole Ni^{II} complex **24**$^-$ as a monoanionic species in the TBA^+ ion pair (Fig. 15a(i)).[56] Here, the stability of the corrole anion was increased by introducing bromo units at the β-positions. Single-crystal X-ray analysis of TBA^+-**24**$^-$ revealed that planar **24**$^-$ and TBA^+ were alternately arranged, forming a columnar structure (Fig. 15a(ii)). Similarly, the octaethylporphyrin Li^I complex **25**$^-$, consisting of monovalent metal and dianionic ligand, behaves as a π-electronic anion (Fig. 15b(i)).[57] **25**$^-$ was synthesized as a $[Li(thf)_4]^+$ (thf = tetrahydrofuran (THF)) ion pair by Li^I metallation of octaethylporphyrin in THF. In $[Li(thf)_4]^+$-**25**$^-$, the components are alternately arranged, and the **25**$^-$ units are inclined to each other (Fig. 15b(ii)). Moreover, $[Li(thf)_4]^+$-**25**$^-$ is sensitive to moisture and undergoes demetallation by hydrolysis.

A variety of charged metal complexes based on neutral π-electronic ligand molecules, such as terpyridine, with another ligand for the partial charge compensation can be used to produce positively charged π-electronic species (*e.g.*, **26**$^+$, Fig. 16a).[58] Terpyridine Pt^{II} complexes with a variety of ligands at Pt^{II} afford planar monocationic species, demonstrating aggregation behaviour using $^i\pi$–$^i\pi$ and Pt^{II}···Pt^{II} interactions.[59] Yam *et al.* reported a terpyridine Pt^{II} complex with an aliphatic alkynyl ligand **26a**$^+$-X^- with different anions (X^- = Cl^-, OTf^-, BF_4^- and PF_6^-), exhibiting luminescence and gelation properties (Fig. 16b(i)).[59b] The OTf^- ion pair formed coil-shaped helical fibres, whereas other ion pairs formed disordered fibres (Fig. 16b(ii)). Furthermore, in 2012, the groups of Che and Yam independently reported a class of monocationic cyclometalated Au^{III} alkynyl complexes **27a,b**$^+$ (Fig. 17a).[60] The positive

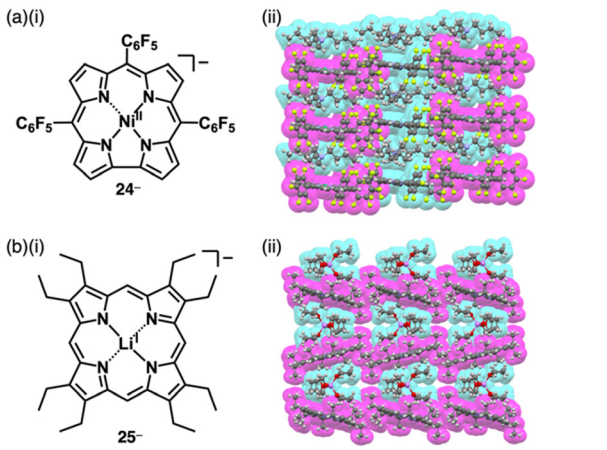

Fig. 15 (a) (i) Corrole Ni^{II} complex **24**$^-$ and (ii) single-crystal X-ray structure of TBA^+-**24**$^-$ and (b) (i) porphyrin Li^I complex **25**$^-$ and (ii) single-crystal X-ray structure of $[Li(thf)_4]^+$-**25**$^-$ ($[Li(thf)_4]^+$ is highlighted with cyan owing to the coordination of THF to Li^+). The crystal structures are redrawn from cif files: 2122003 and 1184624. Atom colour code in (b) (ii) and following figures: light purple in the ball-and-stick models refers to lithium.

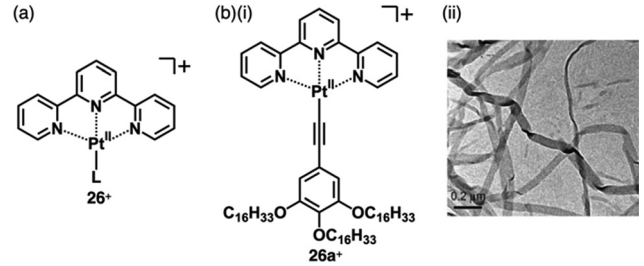

Fig. 16 (a) General structure of positively charged terpyridine Pt^{II} complexes **26**$^+$ and (b) (i) terpyridine Pt^{II} complex with aliphatic chains and (ii) TEM image of the DMSO gel of **26a**$^+$-OTf^- (redrawn from ref. 59b. Copyright 2009 Wiley).

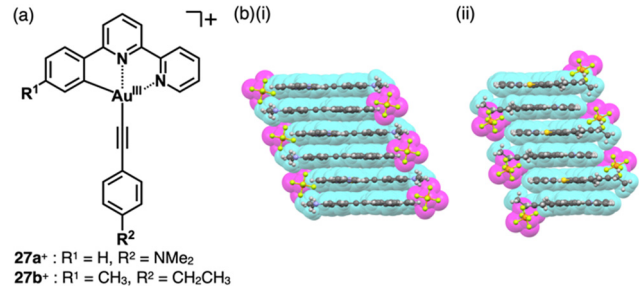

Fig. 17 (a) Positively charged phenylbipyridine Au^{III} complexes **27a,b**$^+$ and (b) single-crystal X-ray structures of (i) **27a**$^+$-PF_6^- and (ii) **27b**$^+$-PF_6^- (redrawn from cif files: 841764 and 897336).

charges of the Au^{III} are partially cancelled by phenylbipyridyl and alkynyl ligands, affording charge-segregated assemblies comprising stacked Au^{III} complexes (Fig. 17b). The short $Au^{III}\cdots Au^{III}$ distances of 3.495 and 3.692 Å in **27a**$^+$-PF_6^- and **27b**$^+$-PF_6^- suggest favourable $Au^{III}\cdots Au^{III}$ interactions as confirmed by theoretical calculations. In **27a**$^+$-PF_6^-, contributions of $^i\pi$–$^i\pi$ and $Au^{III}\cdots Au^{III}$ interactions facilitate the formation of belt-like assemblies.[60a] Tuning of metal centre valences also results in anionic species.[61] Lalinde *et al.* prepared stable anionic Pt^{II} complexes with diphenylpyridine and alkynyl ligands (*e.g.*, **28**$^-$, Fig. 18).[61a] Here, TBA^+ was selected for charge compensation of anionic Pt^{II} complexes. Single-crystal X-ray analysis clearly elucidated the planar geometries of the anionic Pt^{II} complexes, which were further used as guest species for cationic Pt^{II} tweezers, exhibiting more efficient binding behaviour ($\log K$ = 13.5 in CH_2Cl_2) compared to an uncharged Pt^{II} complex.[62]

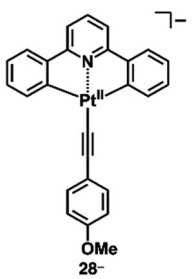

Fig. 18 Negatively charged diphenylpyridine Pt^{II} complex **28**$^-$.

2.3. Charged π-electronic systems formed by protonation and deprotonation

Reversible proton attachment and detachment can be considered covalent approach methods *via* the modulation of covalent linkages (Fig. 1b(iii,iv)). Proton (H^+) is the simplest cation, and protonation of electronically neutral π-electronic systems produces π-electronic cations. The charged π-electronic systems are often deprotonated, reverting neutral π-electronic systems. Thus, π-electronic systems with high proton affinity, achieved by multiple hydrogen bonds, are required to form π-electronic cations suitable for ion pairing.[63,64] Protonated azacalix[3](2,6)pyridine **29a**$^+$ has a cavity with three imine nitrogen sites, exhibiting high basicity (pK_a = 23.1 in CD_3CN) (Fig. 19a(i)).[63a,b] A planar structure with a bound proton in the cavity was investigated by single-crystal X-ray analysis of **29a**$^+$-PF_6^- (Fig. 19a(ii)). A columnar structure of slip-stacked **29a**$^+$ is formed with PF_6^- located at the side of the columns. The basicity is further enhanced by introducing electron-donating pyrrolidine units at the pyridine 4-positions in **29b**$^+$ (pK_a = 28.1 in CD_3CN)), facilitating its application as organocatalysis for Michael addition reactions.[63b] Replacement of the pyridyl units with triazine results in a further electron-deficient π-electronic cation azacalix[3]triazine **30**$^+$ (Fig. 19b(i)), maintaining high basicity (pK_a = 16.7 for the ion pair with **30**$^+$-Cl^- in DMSO).[63d] The protonated species **30**$^+$ interacts with a counteranion, affecting the pK_a values (17.1 and 16.2 for the NO_3^- and PF_6^- ion pairs,

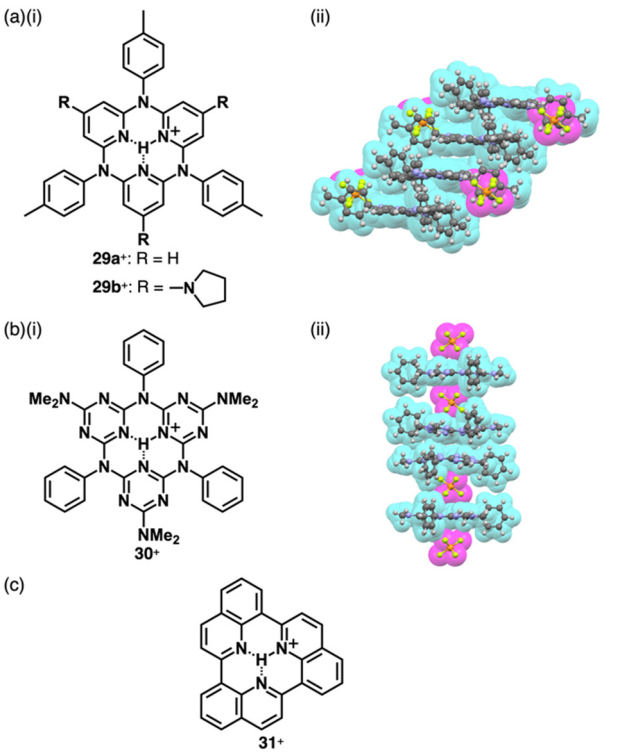

Fig. 19 (a) (i) Protonated azacalix[3](2,6)pyridine **29a,b**$^+$ and (ii) single-crystal X-ray structure of **29a**$^+$-PF_6^- (redrawn from a cif file: 298963), (b) (i) protonated azacalix[3]triazine **30**$^+$ and (ii) single-crystal X-ray structure of **30**$^+$-PF_6^- (redrawn from a cif file: 2072959) and (c) protonated triquinoline **31**$^+$.

respectively, in CD_3CN). Single-crystal X-ray analysis of **30**$^+$-PF_6^- reveals the planar structure of **30**$^+$ with anion–π interactions between PF_6^- and triazine units, resulting in the formation of discrete assemblies in the form of PF_6^--**30**$^+$-PF_6^--**30**$^+$-**30**$^+$-PF_6^--**30**$^+$-PF_6^- (Fig. 19b(ii)). Protonated triquinoline **31**$^+$ (Fig. 19c) possesses a planar rigid skeleton with a proton-binding site, as evidenced by the persistence of >10% of the inner NH ^{1}H NMR signal after one week in CD_3OD.[64] These highly basic macrocycles have been utilized as base catalysts in organic synthesis, and can serve as π-electronic cations in ion-pairing assemblies when paired with suitable anions.

Covalent linkage between charged substituents and π-electronic systems more drastically affects the electronic states of charged π-electronic systems. A ubiquitous negatively charged moiety is O^-, formed by the deprotonation of a hydroxy group. A π-electronic anion precursor is phenol, whose pK_a is 10.00 in an aqueous solution.[65] π-Extended phenol derivatives, such as fluorescein (pK_a = 6.7 for the phenolic OH),[66] whose dianion form is uranine **32**$^{2-}$ (Fig. 20a), are also commercially available as Na^+ salts. Fluorescein derivatives that exhibit pH-dependent photophysical properties are used as pH indicators. Phenoxides are further stabilized by introducing electron-withdrawing groups as seen in picric acid (pK_a of 0.40),[65] providing **33**$^-$ upon deprotonation (Fig. 20b).

4-Nitrophenol (pK_a = 7.14), whose acidity is weaker than picric acid, can be used as a building unit of π-electronic anions. Introduction of pyrrole at the *ortho*-positions of the deprotonated site affords the intramolecular N–H···O$^-$ interactions, which stabilize the π-electronic anions **34a–c**$^-$ (Fig. 21a(i)).[67] The pK_a value of **34b** (7.2) is higher than that of **34a** (6.2), comparable to 4-nitrophenol. In the solid state, TBA$^+$-**34a,b**$^-$ form planar structures, stabilized by intramolecular N–H···O hydrogen bonding. Planar **34a,b**$^-$ are stacked with counter TBA$^+$, providing charge-by-charge columnar assemblies (Fig. 21a(ii)). Introduction of aliphatic alkyl chains at the aryl groups in TBA$^+$-**34c**$^-$ induces liquid crystal mesophases with a Col_h structure based on charge-by-charge assembly, as observed in the crystal structure of TBA$^+$-**34b**$^-$ (Fig. 21a(iii)).[67b] Efforts to introduce electron-withdrawing fluorine at the pyrrole β-positions in search of more stable π-electronic anions yields the desired species. However, handling and purification of this species is challenging owing to its easy deprotonation.[67d] In contrast, introducing thiophene units instead of pyrrole rings affords the π-electronic anion **35a**$^-$, with a pK_a of 6.7 (Fig. 21b(i)).[68] Detailed theoretical studies and single-crystal X-ray analysis of TBA$^+$-**35a**$^-$ revealed intramolecular S···O$^-$ chalcogen bonding (Fig. 21b(ii)). Similarly, TBA$^+$-**35b**$^-$ shows alternate stacking of planar **35b**$^-$ and TBA$^+$ (Fig. 21b(i,iii)). Furthermore, introducing quinone methide units as electron-withdrawing groups and

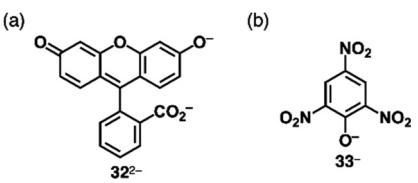

Fig. 20 (a) Uranine **32**$^{2-}$ and (b) deprotonated picric acid **33**$^-$.

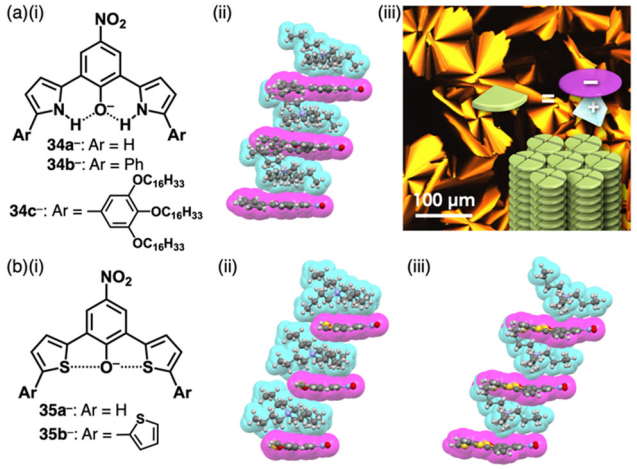

Fig. 21 (a) (i) Deprotonated dipyrrolylnitrophenols **34a–c**$^-$, (ii) single-crystal X-ray structure of TBA$^+$-**34b**$^-$ and (iii) POM image of TBA$^+$-**34c**$^-$ at 65 °C upon cooling (redrawn from ref. 67b. Copyright 2018 Wiley) and (b) (i) deprotonated dithienylnitrophenols **35a,b**$^-$ and single-crystal X-ray structures of (ii) TBA$^+$-**35a**$^-$ and (iii) TBA$^+$-**35b**$^-$. The crystal structures are redrawn from cif files: 1830529, 2253150 and 2253154.

extended π-electronic system effectively stabilizes deprotonated pyrrole units (Fig. 22).[69] Pyrrole-bridged quinone undergoes deprotonation by treatment with tetraalkylammonium hydroxide, inducing a red-shifted absorption band of ~150 nm for **36**$^-$ (Fig. 22a). In TPA$^+$-**36**$^-$ (TPA$^+$: tetrapropylammonium), TPA$^+$ is located on the π-plane of **36**$^-$, inhibiting the stacking of **36**$^-$ (Fig. 22b).

The delocalization of the negative charge is essential to obtain stable π-electronic anions. Deprotonated species of *meso*-hydroxy-substituted porphyrins afford stable π-electronic anionic species **37**$^-$ and **37a–d**$^-$ (Ni^{II}, Zn^{II}, Pd^{II} and Pt^{II} complexes, respectively) (Fig. 23a).[9,70] The pK_a value of **37a** is estimated to be 7.89, higher than those of dipyrrolylnitrophenols **34a,b**. The deprotonated structures of **37a–d**$^-$ as TBA$^+$ ion pairs exhibit the charge-by-charge columnar structures (Fig. 23b(i)). Furthermore, the hydroxy group serving as a directing group enables the selective introduction of phenyl groups at adjacent positions. Treatment of **37a** with $Pd(OAc)_2$, *rac*-BINAP and Cs_2CO_3 yields the Pd-BINAP-complex; further treatment with PhMgBr affords β-phenyl- and diphenyl-substituted **38a,b** (Fig. 23a).[70b] The pK_a values of 8.18 and 8.25 for **38a,b**, respectively, are higher than that of **37a**, confirming the electron-donating nature of the phenyl rings. Upon deprotonation, the ion pairs TBA$^+$-**38a,b**$^-$

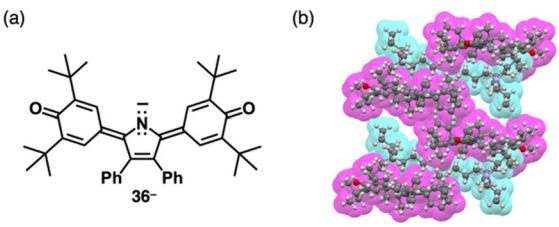

Fig. 22 (a) Deprotonated pyrrole-bridged quinone **36**$^-$ and (b) single-crystal X-ray structure of TBA$^+$-**36**$^-$ (redrawn from a cif file: 2076443).

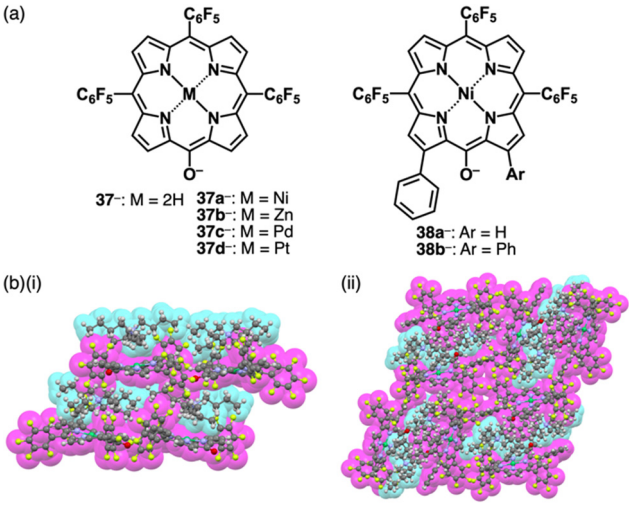

Fig. 23 (a) Deprotonated *meso*-hydroxyporphyrins **37**$^{\bullet-}$ and **37a**–**d**$^{\bullet-}$ (M = Ni, Zn, Pd and Pt) and β-monophenyl **38a**$^{\bullet-}$ and diphenyl-substituted **38b**$^{\bullet-}$ and (b) single-crystal X-ray structures of (i) TBA$^+$-**37a**$^{\bullet-}$ and (ii) TBA$^+$-**38b**$^{\bullet-}$ (redrawn from cif files: 1536339 and 1901215).

form charge-by-charge ion-pairing assemblies in the solid state (Fig. 23b(ii)). The introduction of suitable aryl units allows for the delocalization of the negative charge, resulting in π-extended anionic species with higher stability.

3. π-Electronic systems with charge introduced by noncovalent interactions: ion complexes that sparked π-electronic ion-pairing chemistry

Charge in π-electronic systems can be introduced by noncovalent interactions with inorganic ions, especially, anions (Fig. 1b(v)). Anion binding[71] of anion-responsive π-electronic systems (receptors) leads to the formation of pseudo-π-electronic anions, which are incorporated into ion-pairing assemblies along with π-electronic cations, some of which are discussed in Section 2. Anion binding by π-electronic receptors transforms hard inorganic anions to soft "pseudo-π-electronic" anions, resulting in charge delocalization within the host π-electronic systems (Fig. 24(i)). These formed anion complexes, acting as pseudo-π-electronic anions, can be stacked with π-electronic cations through $^{i}\pi$–$^{i}\pi$ interactions, primarily involving electrostatic and dispersion forces (Fig. 24(ii)). Various pseudo-π-electronic anions can be generated based on the guest anions, with their countercations serving as the counter species of the resulting anion complexes. The stacked pairs of anion complexes and countercations, termed pseudo-π-*sips*, are fundamental building blocks of ion-pairing assemblies. The focus of this section is on the anion complexes of anion-responsive π-electronic molecules, as the chemistry of ion-pairing assemblies originates from the structures assembled with alternately stacked anion complexes and π-electronic cations.[5]

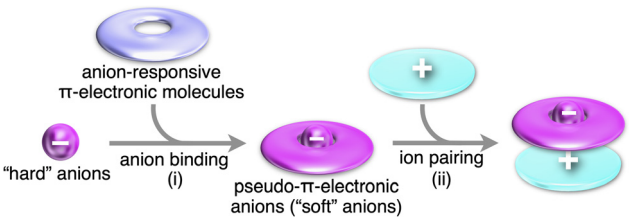

Fig. 24 Conceptual scheme for the formation of π-electronic ion pairs through (i) anion binding and (ii) ion pairing. Pseudo-π-electronic anions as soft anions are obtained by the binding of a hard anion by π-electronic receptors. The pseudo-π-electronic anions form ion pairs in combination with counter π-electronic cations.

3.1. Charged π-electronic systems formed by ion binding

Various types of anion-responsive molecules have been synthesized as colourimetric selective anion sensors and anion transporters in membranes.[71] However, only a few reports discuss planar receptor–anion complexes. The design of anion receptors using π-electronic systems is essential for the formation of planar receptor–anion complexes. Building subunits such as pyrrole and triazole have polarized structures with an H unit that acts as a hydrogen-bonding donor.

As pyrrole-based anion receptors that show planar structures, dipyrrolyldiketone BF_2 complexes (PBs, **39a**–**h** as examples) have two pyrrole units attached to the electron-withdrawing 1,3-propanedione unit (Fig. 25).[5a,72] The pyrrole NH units can be directed to the propanedione CH side by rotating the pyrrole rings, and, in the resulting conformation, the two NH and one CH units serve as anion-binding sites with high binding constants for various anions (K_a = 15 000 M^{-1} for **39a** to bind Cl$^-$ in CH_2Cl_2).[72c] Peripheral modifications at the pyrrole and boron units facilitate further functionalization. A previous review article summarizes representative results in anion-binding and assembling behaviours.[5a] α-Phenyl derivative **39d** (Fig. 25b) shows enhanced anion-binding ability owing to the additional *o*-CH as

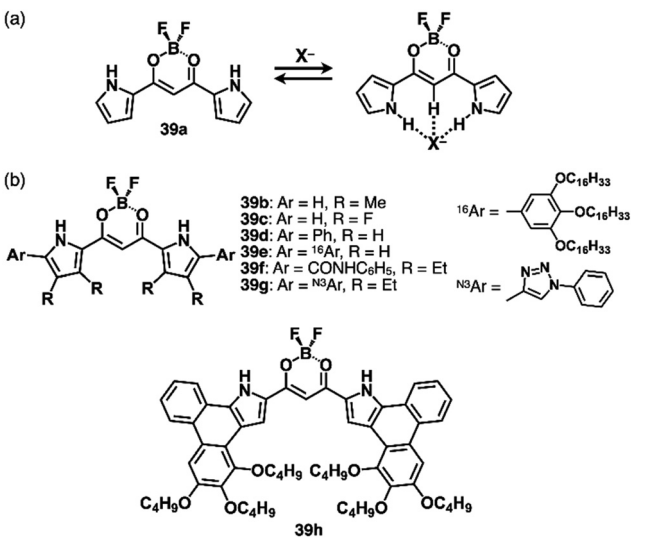

Fig. 25 (a) Anion-binding behaviour of dipyrrolyldiketone BF_2 complex (PB) **39a** and (b) PB derivatives **39b**–**h**.

supportive interaction sites.[72b] Single-crystal X-ray analysis of TPA$^+$-**39d**·Cl$^-$ clearly demonstrates the planar geometry of **39d**·Cl$^-$. Importantly, the planar **39d**·Cl$^-$ and counter TPA$^+$ are alternately stacked, forming a charge-by-charge columnar structure. The discovery of ion-pairing assemblies with alternately stacked anion complexes and π-electronic cations sparked the idea of incorporating planar countercations (*vide infra*, Section 3.2).

Efficient anion-binding behaviours of PB have been applied for inducing further functionalities (Fig. 25b). Modifications of the α-positions such as α-amide-substituted **39f** exhibit higher anion-binding behaviour ($K_a \geq 10^8$ M^{-1} for Cl$^-$ in CH_2Cl_2) to form solid-state ion-pairing assemblies.[72g] Moreover, click reactions of an α-diethynyl-substituted receptor[72f] and arylazides afford triazole-substituted receptors including **39g**.[72l] The triazole-CH functions as an anion-binding site, forming planar receptor–anion complexes in ion-pairing assemblies. Covalently linked PB dimers show high anion-binding affinities by forming helical structures as building blocks of ion-pairing assemblies.[72d,e,73] OFF–ON fluorescence switching by anion binding has been demonstrated in hexaaryl-substituted PB derivatives based on anion-dependent intramolecular photo-induced electron transfer (PET), demonstrating potential logic gate systems.[72j,k] More efficient anion-binding and ion-pairing behaviours can be achieved by including the PB unit in the macrocycles owing to pyrrole-inverted preorganized structures.[72h]

Shape-persistent macrocycles with preorganized anion-binding structures based on π-electronic subunits facilitate the preparation of planar receptor–anion complexes.[74] Flood *et al.* synthesized a triazolophane anion receptor **40** (Fig. 26), containing polarized aryl-CH units as interaction sites, providing an anion-binding cavity.[75] By exclusively employing aryl-CH units, **40** demonstrates a highly efficient anion-binding capability (K_a = 4 700 000 M^{-1} for Cl$^-$ in CH_2Cl_2). Moreover, **40** forms stacked [2+1]-type anion complexes with larger anions, such as I$^-$, through the effective π–π stacking of the aromatic units present in **40**.

Cyanostar (CS) **41**, serving as another planar π-electronic anion receptor, incorporates five electron-withdrawing cyano groups, making the inner CH units highly efficient hydrogen-bonding donors (Fig. 26).[76] Owing to the presence of an internal anion-binding cavity with five CH units, CS exhibits high binding constants for larger anions, including BF_4^-, PF_6^- and ClO_4^- ($\log K_a \sim 5$). [2+1]-Type anion complexes for larger anions based on effective π–π stacking of CS serve as key structures for fabricating ion-pairing assemblies.

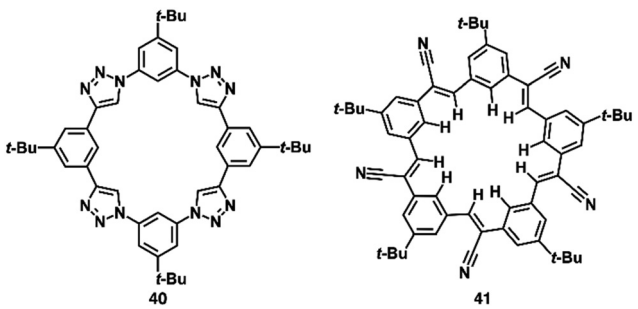

Fig. 26 Macrocyclic anion receptors: triazolophane **40** and cyanostar (CS) **41**.

3.2. π-Electronic ion-pairing assemblies comprising anion receptors

Since the initial discovery of the solid-state charge-by-charge assembly of TPA$^+$-**39d**·Cl$^-$, as illustrated in Section 3.1, there has been a trend of introducing more planar countercations instead of the bulky ammonium cations for the formation of charge-by-charge assemblies. In our preliminary trial for the use of planar countercations, tris(diethylamino)-substituted TOTA$^+$ [15b] was incorporated in the solid-state charge-by-charge assembly with the anion complex of **39d**. Because of the difficulty in excluding I$^-$ from the starting ion pair TOTA$^+$-Cl$^-$ by anion exchange protocol, other suitable π-electronic cations have been explored to fabricate ion-pairing assemblies. For example, ^{3}TATA$^+$-Cl$^-$, which can be synthesized from the Cl$^-$ salt a tritylium derivative, was used for an alternative π-electronic cation.[7] Planar **39d**·Cl$^-$ and ^{3}TATA$^+$ formed a charge-by-charge assembly *via* ^{i}π–^{i}π interactions, with a shorter stacking distance than that of TPA$^+$-**39d**·Cl$^-$ (Fig. 27a). Furthermore, ^{3}TATA$^+$-**39e**·Cl$^-$ with aliphatic alkyl chains forms a supramolecular gel comprising micrometre-scale fibrous morphologies (Fig. 27b). X-ray diffraction analysis of the xerogel revealed the formation of a Col$_h$ structure with a diffraction peak at 0.74 nm, which is nearly twice of π–π stacking distances. This distance was assigned as the repeating distance of identically charged species in the charge-by-charge assembly. In addition, ^{3}TATA$^+$-**39e**·Cl$^-$ forms a liquid crystal mesophase based on the Col$_h$ packing of charge-by-charge assembly.[7]

Moreover, porphyrin Au^{III} complexes have been used as countercations of π-electronic ion-pairing assemblies comprising PB-based anion complexes. For example, in the crystal structure of **22a**$^+$-**39a**·Cl$^-$, a stacked **22a**$^+$ dimer was sandwiched by planar **39a**·Cl$^-$ (Fig. 28a).[77] In contrast, in **22a**$^+$-**39b**·Cl$^-$, **22a**$^+$

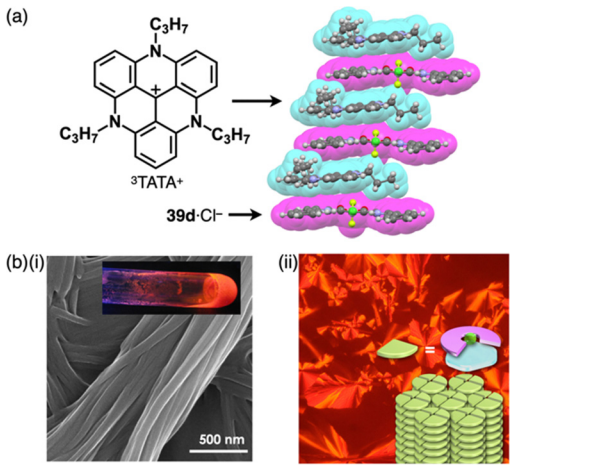

Fig. 27 (a) Single-crystal X-ray structure of ^{3}TATA$^+$-**39d**·Cl$^-$ (redrawn from a cif file: 745780) and (b) (i) photograph and SEM of the supramolecular gel and (ii) POM and packing model of the liquid crystal mesophase of ^{3}TATA$^+$-**39e**·Cl$^-$ (redrawn from ref. 7. Copyright 2010 Wiley).

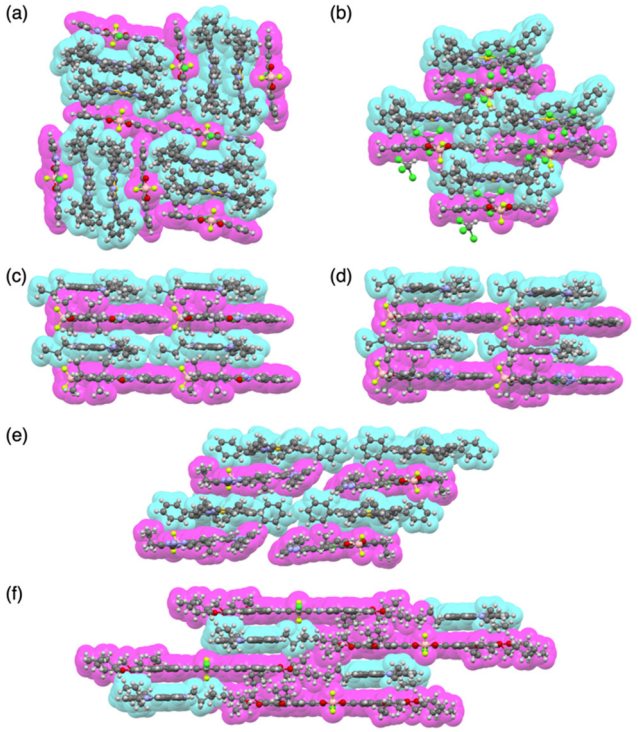

Fig. 28 Single-crystal X-ray structures of (a) **22a**$^+$-**39a**·Cl$^-$, (b) **22a**$^+$-**39b**·Cl$^-$, (c) ^{3}TATA$^+$-**39f**·Cl$^-$, (d) ^{3}TATA$^+$-**39g**·Cl$^-$, (e) **22a**$^+$-**39g**·Cl$^-$ and (f) ^{3}TATA$^+$-**39h**·Cl$^-$ (redrawn from cif files: 1969168, 1969169, 1546127, 213826, 213827 and 1900650).

and planar **39b**·Cl$^-$ are alternately stacked with a π–π stacking distance (Fig. 28b). **22a**$^+$-**39c**·Cl$^-$ forms a similar charge-by-charge assembly. Furthermore, charge-by-charge assemblies of ^{3}TATA$^+$-**39f**·Cl$^-$, ^{3}TATA$^+$-**39g**·Cl$^-$ and **22a**$^+$-**39g**·Cl$^-$ have been observed (Fig. 28c–e). Effective stacking of the planar receptor–anion complex and countercation is supported by EDA, suggesting a cooperative contribution of electrostatic and dispersion forces in the stacked ion pairs of ^{3}TATA$^+$-**39g**·Cl$^-$ and **22a**$^+$-**39g**·Cl$^-$.[72l] Furthermore, π-extended PB **39h** exhibits a planar [1+1]-type Cl$^-$ complex, showing the stacking with ^{3}TATA$^+$ in the solid state (Fig. 28f).[72i]

Recent studies based on the crystal analysis have revealed a variety of charge-by-charge assemblies depending on the constituting receptor–anion complexes and π-electronic countercations. **42** forms a planar [2+1]-type anion complex **42**$_2$·Cl$^-$ in the crystal structure of ^{3}TATA$^+$-**42**$_2$·Cl$^-$, where the layers of identically charged species are alternately stacked (Fig. 29a).[78] Furthermore, introducing naphthalenediolate units instead of two fluorine moieties at the boron unit affects the assembling modes.[79] In the assembly of the naphthalene-2,3-diolate boron complex as a ^{3}TATA$^+$ ion pair ^{3}TATA$^+$-**43a**·Cl$^-$, the stacked ^{3}TATA$^+$ dimer is sandwiched by the naphthyl unit of **43a**·Cl$^-$. Conversely, in ^{3}TATA$^+$-**43b**·Cl$^-$, alternately stacked ^{3}TATA$^+$ and the receptor–Cl$^-$ complex unit in **43b**·Cl$^-$ are observed (Fig. 29b). Square planar dipyrrolyldiketone Pt^{II} complexes that have phenylpyridine as another ligand part are also suitable for stacking assemblies (Fig. 30a).[80] In the crystals of Pt^{II} complex ion pairs **22c**$^+$-**44a**·Cl$^-$

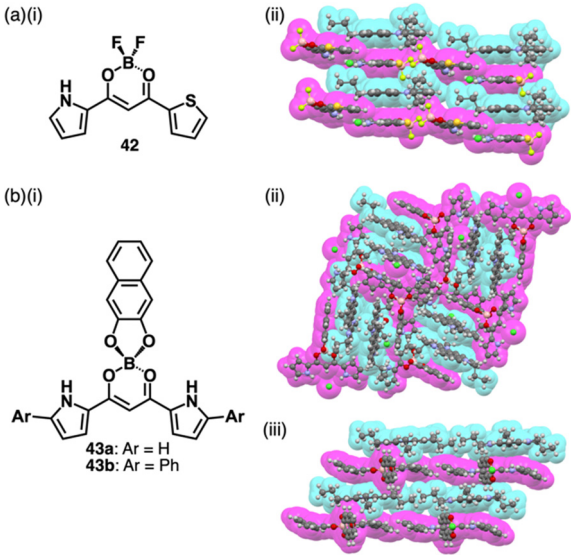

Fig. 29 (a) (i) Pyrrolylthienyldiketone BF_2 complex **42** and (ii) single-crystal X-ray structure of ^{3}TATA$^+$-**42**$_2$·Cl$^-$ and (b) (i) naphthalenediolate boron complexes **43a,b** and (ii) single-crystal X-ray structures of ^{3}TATA$^+$-**43a**·Cl$^-$ and (iii) ^{3}TATA$^+$-**43b**·Cl$^-$. The crystal structures are redrawn from cif files: 1840326, 2227398 and 2227399.

and **22a**$^+$-**44b**·Cl$^-$, Au^{III} complexes and anion complexes are alternately stacked and form columnar structures (Fig. 30b). These solid-state charge-by-charge assemblies, comprising the anion complexes of PB and Pt^{II} complexes, demonstrate the potential to induce diverse assembling modes and resulting properties based on neutral receptor units.

In the ion-pairing assemblies of CS, the **4a**$^+$-**41**$_2$·BF_4^- ion pair is stacked with another ion pair, forming a charge-by-charge assembly, exhibiting a distinct red-shifted emission band derived from **4a**$^+$, in a concentrated solution (0.2 mM) as well as crystalline and film states.[76b] Various cationic dyes can be introduced as the countercations of ClO_4^-, and the ion pairs form charge-by-charge assemblies in the crystalline state, as shown in **45a**$^+$-**41**$_2$·ClO_4^- (Fig. 31a and b).[76c] Usually, crystal-state photophysical properties, different from those in solution, are affected by exciton coupling depending on the arrangement

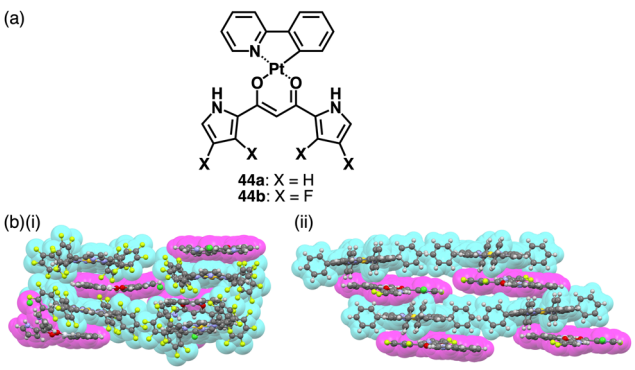

Fig. 30 (a) Dipyrrolyldiketone Pt^{II} complexes **44a,b** and (b) single-crystal X-ray structures of (i) **22c**$^+$-**44a**·Cl$^-$ and (ii) **22a**$^+$-**44b**·Cl$^-$ (redrawn from cif files: 2063433 and 2063434).

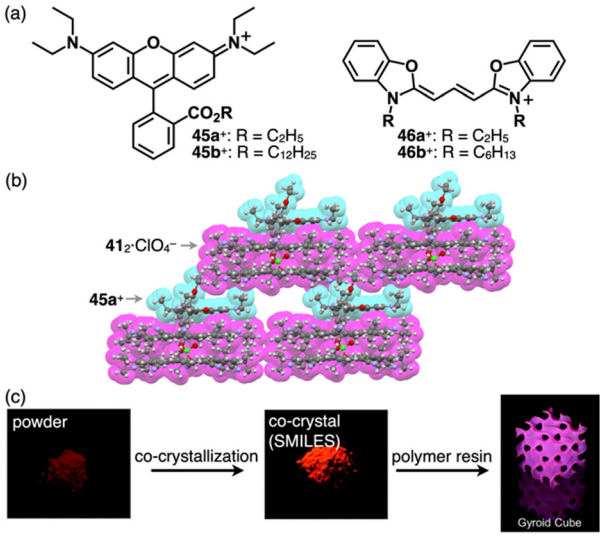

Fig. 31 (a) Rhodamines **45a,b**$^+$ and cyanines **46a,b**$^+$, (b) single-crystal X-ray structure of **45a**$^+$-**41**$_2$·ClO_4^- (redrawn from a cif file: 1895155) and (c) photographs of **45a**$^+$ (left), **45a**$^+$-**41**$_2$·ClO_4^- (centre) and **45a**$^+$-**41**$_2$·ClO_4^- contained in polymer resin (right) (redrawn from ref. 76c. Copyright 2020 Elsevier).

of π-electronic molecules. In contrast, the cationic dyes within the charge-by-charge assemblies with CS anion complexes are spatially and electronically isolated, and the exciton coupling is suppressed. Flood *et al.* proposed charge-by-charge assemblies as small-molecule ionic isolation lattices (SMILES). Ensuring that the frontier molecular orbitals of the cationic dyes are located inside those of the anion complex of CS is crucial. Using SMILES, the polymer resin containing **45a**$^+$-**41**$_2$·ClO_4^- exhibits an emissive solid-state material (Fig. 31c).[76c] Furthermore, **45b**$^+$-**41**$_2$·PF_6^- forms SMILES-based nanoparticles, exhibiting bright emission derived from **45b**$^+$ upon excitation of **41**$_2$·PF_6^- owing to the effective energy transfer (φ_{ET} = 80%) between the oppositely charged π-electronic systems.[76d] A similar phenomenon was observed in the nanoparticles of **46b**$^+$-**41**$_2$·PF_6^-.[76e] In particular, the energy transfer efficiency of **46b**$^+$-**41**$_2$·PF_6^- reaches 100% owing to the larger overlap of emission of **41**$_2$·PF_6^- and the absorption bands of the cationic dye. However, the fluorescence quantum yield of SMILES is low (12.8%), owing to Förster resonance energy transfer to dark trap states or reabsorption. The deactivation path is suppressed by doping fluorescent dyes into SMILES comprising cationic dyes with higher excitation energies, drastically improving the fluorescent quantum yields (65% and 29% for **45a**$^+$-ClO_4^--doped and pristine SMILES comprising **46a**$^+$-PF_6^-, respectively).[76f]

4. π-Electronic ion pairs: pairs of π-electronic cations and anions

The π-electronic cations described in Section 2 are introduced as the counter species for the anion complexes of anion-responsive π-electronic molecules (Section 3). The combination of π-electronic cations with π-electronic anions, as summarized in Section 2, provides a variety of ion pairs and assemblies. π-Electronic ion pairs are prepared by ion-pair metathesis from desired π-electronic ions with corresponding inorganic counterions.[5b] Ion-pair metathesis, a key procedure for producing π-electronic ion pairs, is derived from the hard and soft acids and bases (HSAB) theory, which requires hard ions such as Cl^- and Na^+ for desired cation and anions, respectively, in starting materials (Fig. 32). For categorizing and summarizing π-electronic ion pairs, this section focuses on the types of π-electronic anions, which are relatively difficult to prepare than π-electronic cations owing to their reactivity.

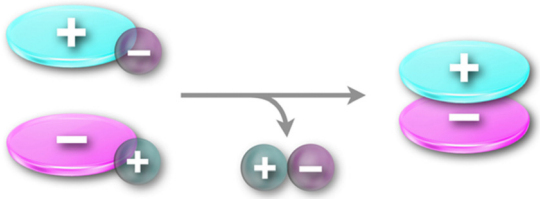

Fig. 32 Ion-pair metathesis for the preparation of π-electronic ion pairs.

4.1. π-Electronic ion pairs comprising cyclopentadienide-based π-electronic anions

Photophysical properties and ion-pairing assemblies of π-electronic ion pairs were investigated based on cyclopentadienide **13**$^-$.[81] In 1963, ion pairs of **13**$^-$ were prepared by ion-pair metathesis of K^+-**13**$^-$ and various π-electronic cations, such as Tr^+ and **47**–**49**$^+$ as BF_4^- salts (Fig. 33a).[81a] The ion pairs exhibit countercation-dependent CT bands. The CT band of Tr^+-**13**$^-$ is blue-shifted in polar solvents (474 and 439 nm in CH_2Cl_2 and MeOH, respectively) with a smaller solvent dependence than Tr^+-I^- (571 and 403 nm, respectively).[81b] Alternately arranged Tr^+ and **13**$^-$ form a charge-by-charge assembly in the crystal structure (Fig. 33b).[81d] The CT absorption band of an *N*-methylpyridinium ion pair **49a**$^+$-**13**$^-$ at −170 °C in a MeOH/EtOH glassy solution was observed (λ_{abs} ∼ 340 nm as a shoulder); compared to other ion pairs with Br^-, N_3^-, SCN^- and I^-, it was red-shifted, whereas the emission band was blue-shifted.[81c]

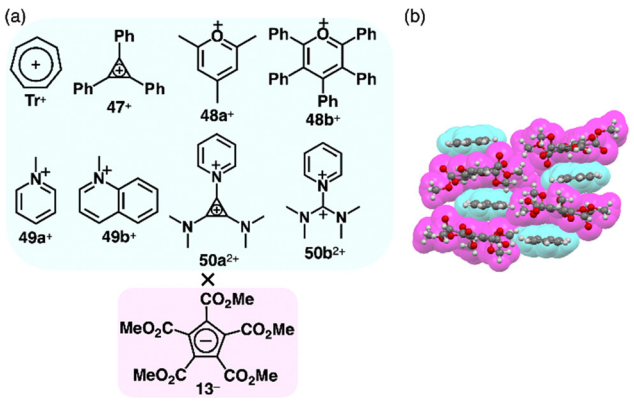

Fig. 33 (a) π-Electronic ion pairs of pentamethoxycarbonyl-substituted cyclopentadienide **13**$^-$ with π-electronic cations Tr^+, **47**–**49**$^+$ and **50a,b**$^{2+}$ and (b) single-crystal X-ray structure of Tr^+-**13**$^-$ (redrawn from a cif file: 1141949).

Therefore, the Stokes shift of **49a**$^+$-**13**$^-$ (1.1×10^4 cm^{-1}) is smaller than those of the other ion pairs ($>1.55 \times 10^4$ cm^{-1}), ascribed to the smaller structural relaxation in the excited state. Ion pairs of dicationic **50a**$^{2+}$ and **13**$^-$, **50a**$^{2+}$-**13**$^-$-X$^-$ (X$^-$ = OTf$^-$ and BF_4^-) and **50a**$^{2+}$-**213**$^-$, were prepared by the ion-pair metathesis of **50a**$^{2+}$-2X$^-$ and K$^+$-**13**$^-$.[81e] Similarly, **50b**$^{2+}$ provided ion pairs with **13**$^-$ in the presence and absence of BF_4^- by the ion-pair metathesis between **50b**$^{2+}$-2BF_4^- and K$^+$-**13**$^-$. The ion pairs of **50a**$^{2+}$ exhibit concentration-dependent CT bands (λ_{abs} = 406 and 424 nm at 1.65 and 3.30 M, respectively, in MeCN for **50a**$^{2+}$-**213**$^-$). In addition, ^{1}H NMR signals of **50a**$^{2+}$-2OTf$^-$ are shifted upfield in the presence of K$^+$-**13**$^-$, suggesting an interaction between **13**$^-$ and **50a**$^{2+}$. In the crystal structure of **50a**$^{2+}$-**13**$^-$-BF_4^-, the dication and **13**$^-$ are alternately stacked on the cyclopropenyl unit rather than the pyridinium unit, forming a charge-by-charge assembly with BF_4^-, located between the columns.[81e] The CO_2Me groups in **13**$^-$ are distorted from the cyclopentadienide core owing to their steric repulsion.[81d,e]

The planar structure of PCCp$^-$ is suitable for more effective stacking of oppositely charged species in combination with π-electronic cations (Fig. 34a). An ion pair of PCCp$^-$ with trityl cation **1**$^+$ was prepared as the precursor of triethylsilyl PCCp$^-$ by the ion-pair metathesis of **1**$^+$-Br$^-$ and Ag$^+$-PCCp$^-$.[82] **1**$^+$ and PCCp$^-$ afforded a columnar structure comprising identically charged species in a crystalline state (Fig. 34b(i)). PCCp$^-$ is stacked with another PCCp$^-$ at an interplanar distance of 3.42 Å to form a pair, which is slip-stacked with other pairs at the cyano groups.[82] In **2**$^+$-PCCp$^-$, **2**$^+$ and PCCp$^-$ are alternately stacked at the two aminophenyl units of **2**$^+$ (Fig. 34b(ii)).[33] Meanwhile, the other aminophenyl group is stacked with the corresponding part of the neighbouring **2**$^+$, resulting in a partially charge-segregated assembly. Meanwhile, the propeller geometries of triarylmethyliums inhibits effective stacking, resulting in the limited contact with the oppositely charged species. On the other hand, PCCp$^-$ in π-electronic ion pairs with more planar π-electronic cations such as Tr$^+$ and ^{3}TATA$^+$ is effectively stacked with the countercations. In Tr$^+$-PCCp$^-$, Tr$^+$ and PCCp$^-$ are alternately stacked to afford a charge-by-charge assembly (Fig. 34b(iii)). In contrast, in ^{3}TATA$^+$-PCCp$^-$, ^{3}TATA$^+$ and PCCp$^-$ are stacked with the respective identically charged species to form stacked dimers, resulting in a two-by-two charge-by-charge assembly (Fig. 34b(iv)).[33] The ion pair of PCCp$^-$ with **51**$^+$, an isoelectronic cation of TATA$^+$ with a B–N unit in place of a central C–C unit, was also prepared by ion-pair metathesis of **51**$^+$-OTf$^-$ and Na$^+$-PCCp$^-$.[83] The crystal structure resembles that of ^{3}TATA$^+$-PCCp$^-$, although each component is slip-stacked with the identically charged species (Fig. 34b(v)). Notably, ^{3}TATA$^+$ and **51**$^+$ are stacked with PCCp$^-$ in relatively short contact (3.29 and 3.25 Å, respectively).

Porphyrin Au^{III} complexes, which are discussed in Sections 2.2 and 3.2, have been adopted as the components of π-electronic ion pairs, as seen in **22a**$^+$-PCCp$^-$.[52] The ion pair forms a solid-state charge-by-charge assembly with the interplanar distances of 3.37 and 3.40 Å (Fig. 34b(vi)).[52a] **22e**$^+$-PCCp$^-$ is also included in a similar charge-by-charge assembly, where the two free *meso*-positions are in contact with PCCp$^-$ CN units.[52b] Conversely, **22c**$^+$-PCCp$^-$ forms a one-by-two charge-by-charge assembly with another **22c**$^+$ unit located between the columns. Asymmetric heteroatom-containing porphyrin analogues with chalcogen elements has been adopted as the countercation of PCCp$^-$. 21-Thiaporphyrin Ni^{II} complex ion pair **23**$^+$-PCCp$^-$ was prepared by ion-pair metathesis of **23**$^+$-Cl$^-$ and Na$^+$-PCCp$^-$.[55] In the crystal structure of **23**$^+$-PCCp$^-$, the thiophene unit of **23**$^+$ is inclined by 24.5°. The **23**$^+$ units are stacked by themselves in antiparallel orientation to form a dimer *via* chalcogen bonding between the thiophene and adjacent pyrrole

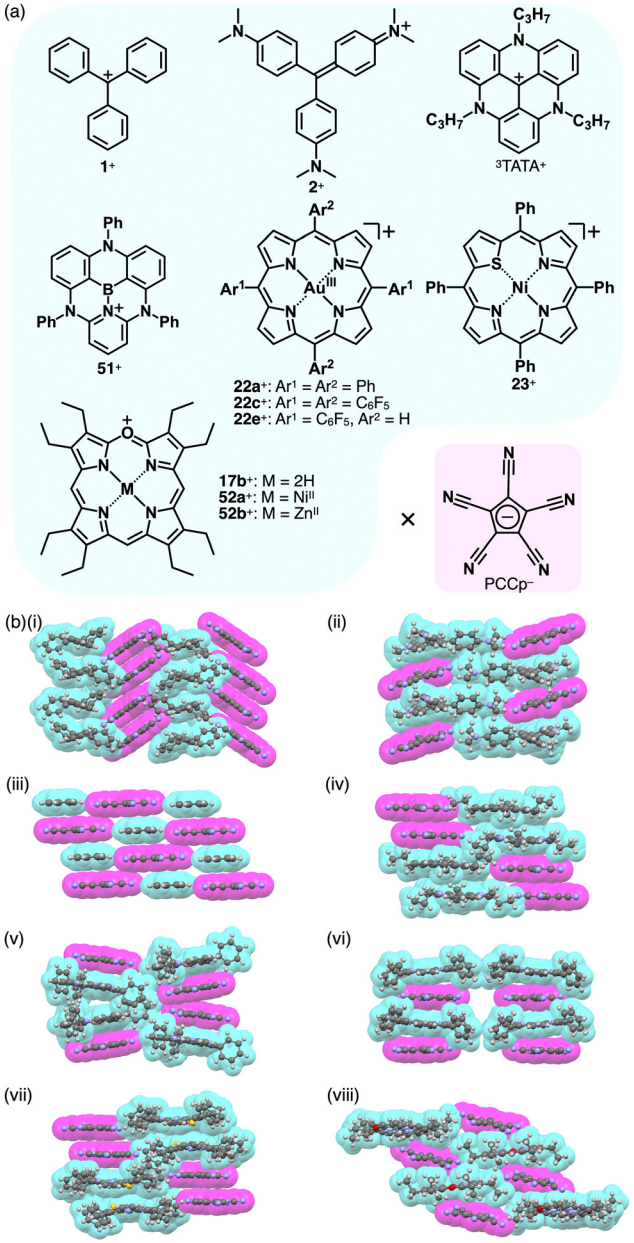

Fig. 34 (a) Combinations of π-electronic ion pairs: PCCp$^-$ with **1**$^+$, **2**$^+$, ^{3}TATA$^+$, BN-TATA **51**$^+$, **22a,c,e**$^+$, **23**$^+$, **17b**$^+$ and **52a,b**$^+$ and (b) single-crystal X-ray structures of (i) **1**$^+$-PCCp$^-$, (ii) **2**$^+$-PCCp$^-$, (iii) Tr$^+$-PCCp$^-$, (iv) ^{3}TATA$^+$-PCCp$^-$, (v) **51**$^+$-PCCp$^-$, (vi) **22a**$^+$-PCCp$^-$, (vii) **23**$^+$-PCCp$^-$ and (viii) **52b**$^+$-PCCp$^-$ (redrawn from cif files: 227124, 1431734, 1431733, 1431735, 2063989, 1877990, 2167304 and 2144318). Atom colour code in (viii): violet in the ball-and-stick models refers to zinc.

units at short S···N distances of 3.26 and 3.33 Å. In addition, $PCCp^-$ forms a stacked dimer, providing a two-by-two charge-by-charge assembly (Fig. 34b(vii)).[55] Similarly, in the $PCCp^-$ ion pair with oxaporphyrin Ni^{II} complex **52a**$^+$, the constituent ions form the respective stacked dimers with interplanar distances of 3.31 and 3.28 Å, respectively.[84] Besides, $PCCp^-$ ion pairs of free-base **17b**$^+$ and Zn^{II} complex **52b**$^+$ form one-by-one charge-by-charge assemblies. In contrast to the almost parallel arrangement observed in **17b**$^+$ and $PCCp^-$, in the ion pair **52b**$^+$-$PCCp^-$, the components are not arranged in parallel owing to the coordination of $PCCp^-$ CN to the Zn^{II} centre (Fig. 34b(viii)).

The introduction of aliphatic alkyl chains into charged π-electronic species induces various soft materials based on ion-pairing assemblies. The porphyrin Au^{III} complex bearing hexadecyloxy chains at the *meso*-aryl moieties **22f**$^+$ provides supramolecular gels and discotic columnar liquid crystals, whose assembled structures depend on the counteranions (Fig. 35).[52a] **22f**$^+$-$PCCp^-$ forms a supramolecular octane gel (10 mg mL^{-1}), owing to the entanglement of fibrous morphologies with diameters of 1–3 μm and lengths exceeding 100 μm (Fig. 35b(i)). Conversely, **22f**$^+$-$PCCp^-$ exhibits a liquid crystal mesophase (36–293 °C) based on the Col_h structure of the charge-by-charge assembly, as observed in the crystal structure of **22a**$^+$-$PCCp^-$ (mentioned earlier) (Fig. 35b(ii)). Meanwhile, **22f**$^+$-Cl^- forms a Col_h structure with charge-segregated assembly, excluding the nonplanar anion from the stacked structure of **22f**$^+$. These findings suggest that the size of $PCCp^-$ complements the core part of porphyrin Au^{III} complexes, facilitating the formation of charge-by-charge assemblies. Notably, the charge-by-charge assembly of **22g**$^+$-$PCCp^-$, which possesses icosyloxy chains, shows anisotropic alignment after shearing. The alignment persists after thermal phase transitions, indicating a robust packing state of charge-by-charge assemblies.[52a]

In the previous paragraphs in this section, the π-electronic ion pairs of $PCCp^-$ form the charge-by-charge assemblies, some of which comprise the stacked dimers of $PCCp^-$ and those of the cations. As seen in the ion pairs with bulky cations, stacking

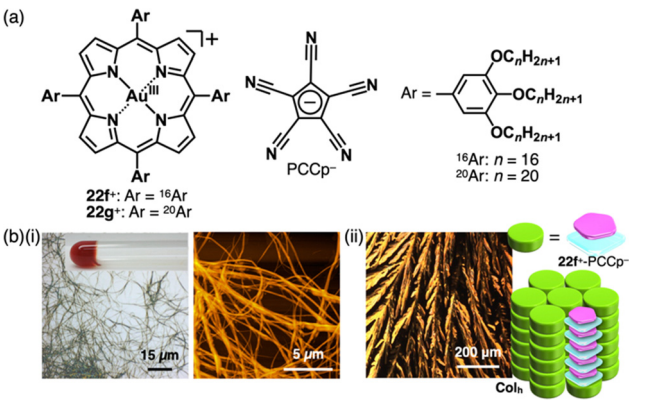

Fig. 35 (a) Ion pair of aliphatic porphyrin Au^{III} complex **22f**$^+$ with $PCCp^-$ and (b) (i) optical microscope and atomic force microscope images of **22f**$^+$-$PCCp^-$ octane gel (10 mg mL^{-1}) and (ii) mesophase properties of **22f**$^+$-$PCCp^-$: POM and a proposed assembled model at 280 °C upon cooling from the isotropic liquid state (redrawn from ref. 52a. Copyright 2019 Elsevier).

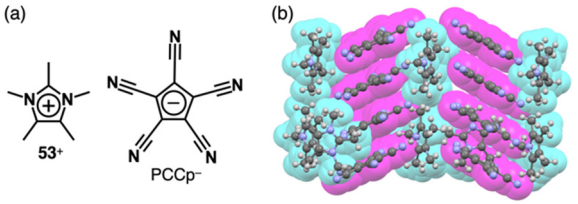

Fig. 36 (a) Ion pair of pentamethylimidazolium **53**$^+$ with $PCCp^-$ and (b) single-crystal X-ray structure of **53**$^+$-$PCCp^-$ (redrawn from a cif file: 1868291).

structures of $PCCp^-$ can be realized by combining π-electronic cations that aggregate independently. For instance, in the crystal structure of the ion pair comprising $PCCp^-$ with pentamethylimidazolium **53**$^+$, $PCCp^-$ is stacked with another $PCCp^-$, leading to a charge-segregated assembly (Fig. 36).[85] In this arrangement, **53**$^+$ is located between the $PCCp^-$ columns without participating in the stacking. Despite the absence of long alkyl chains, the crystal of **53**$^+$-$PCCp^-$ undergoes a phase transition and transforms to the mesophase in a temperature range of 234–240 °C. Interestingly, the ion pair, especially when doped with Na^+-$PCCp^-$, exhibits ionic conductivities.

Charge-segregated assemblies based on stacked structures of $PCCp^-$ and those of π-electronic cations can be constructed by introducing the cationic species that induce specific interactions. The dipole of cationic squarylium **10**$^+$ can be used for stacking in the $PCCp^-$ ion pair (Fig. 37a).[23] The photophysical properties of **10**$^+$-$PCCp^-$ vary with the stacking modes, forming J- and H-aggregates in 1% CH_2Cl_2/*n*-hexane and 1% acetone/water, respectively, while a monomeric state is observed in CH_2Cl_2 (Fig. 37b). Additionally, J-aggregates are formed in chiral media (0.33% to 1% CH_2Cl_2/α- and β-pinene) and exhibit CD signals, indicating the formation of chiral assemblies. These findings highlight the sensitivity of ion-pairing behaviour to the surrounding environment, offering potential applications in chiral recognition and sensing. **10**$^+$-$PCCp^-$ gives two crystal pseudo-polymorphs: (i) a charge-segregated assembly (**10**$^+$-$PCCp^-_{CS}$) (Fig. 37c(i)) and (ii) a partially charge-segregated assembly (**10**$^+$-$PCCp^-_{SS}$) (Fig. 37c(ii)), where **10**$^+$ is partially slip-stacked; hence, the direct contact of identically charged species is smaller than that of **10**$^+$-$PCCp^-_{CS}$. The EDA of the **10**$^+$-$PCCp^-_{CS}$ packing structure indicates that electrostatic force in a stacked pair of **10**$^+$ (c2–c3 in Fig. 37d), oriented in an antiparallel fashion, is smaller than that in a separated pair of **10**$^+$ (c1–c3 in Fig. 37d). The peculiar electrostatic forces contributing to the characteristic assembling behaviour are ascribed to dipole–dipole interactions between identically charged species. Solid-state absorption spectra of the **10**$^+$ ion pairs exhibit counteranion-dependent bands derived from the exciton coupling between stacked **10**$^+$ units. Flash-photolysis (FP) TRMC measurements of the crystalline states of **10**$^+$-$PCCp^-_{CS}$ and **10**$^+$-$PCCp^-_{SS}$ reveal that the former exhibits higher electric conductivity ($\varphi\sum\mu = 3.0 \times 10^{-8}$ m^2 V^{-1} s^{-1}, where φ is the photocarrier generation yield and $\sum\mu$ is the sum of hole and electron mobilities) than the latter ($\varphi\sum\mu = 1.0 \times 10^{-8}$ m^2 V^{-1} s^{-1}), confirming the effective electric conducting properties in the charge-segregated assembly (Fig. 37e). Moreover, **10**$^+$-$PCCp^-_{CS}$

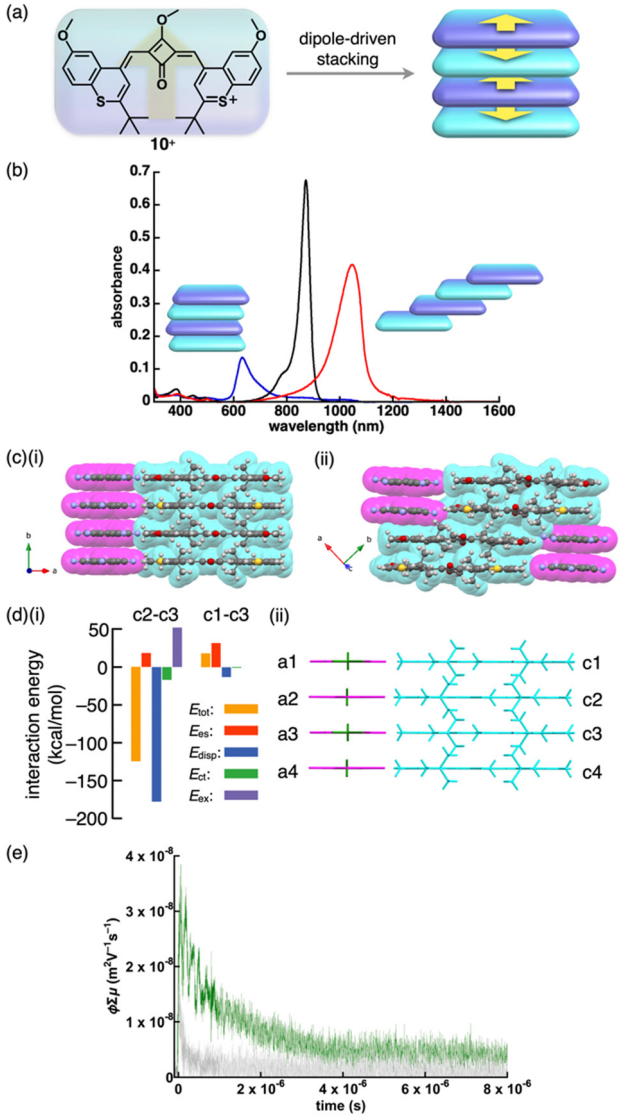

Fig. 37 (a) Conceptual illustration of $\mathbf{10}^+$ with dipole, which induces stacking of identically charged species, (b) UV/vis absorption spectra of $\mathbf{10}^+$-PCCp$^-$ in CH_2Cl_2 (black), dispersed in 1% CH_2Cl_2/*n*-hexane (red) and 1% acetone/water (blue), (c) single-crystal X-ray structures of (i) $\mathbf{10}^+$-PCCp$^-_{CS}$ and (ii) $\mathbf{10}^+$-PCCp$^-_{SS}$ (redrawn from cif files: 2214020 and 2214021), (d) (i) decomposition of the total intermolecular interaction energies of $\mathbf{10}^+$-PCCp$^-_{CS}$ for (ii) the single-crystal X-ray structure with labels and (e) photoconductivity transients observed upon excitation at 355 nm, 9.1 × 10^{15} photons cm^{-2} pulse^{-1} for distinctive single crystals of $\mathbf{10}^+$-PCCp$^-$ as distinctive pseudo-polymorphs of $\mathbf{10}^+$-PCCp$^-_{CS}$ (green) and $\mathbf{10}^+$-PCCp$^-_{SS}$ (light grey) along the long axes of crystals (redrawn from ref. 23. Copyright 2023 Wiley).

exhibits anisotropic electric conductivity along the stacking direction (*b* axis in Fig. 37c(i)).[23]

4.2. π-Electronic ion pairs comprising azolate-based π-electronic anions

The replacement of CHs with electronegative nitrogens in cyclopentadienides enhances their stability, allowing for the production of various π-electronic anions, even with electron-donating groups. Azolium–azolate ion pairs, investigated by Shreeve *et al.*, serve as energetic ionic liquids, finding applications as propellants owing to their explosive nature.[86,87] Ionic liquid ion pairs, such as ethylmethylimidazolium (EMIm$^+$) with 1,2,4-triazolate and tetrazolate, were synthesized using EMIm$^+$-OH$^-$.[87a] Their glass transition temperatures vary based on the constituents. Additionally, the π-electronic ion pair of butylmethylimidazolium 3,5-dinitro-1,2,4-triazolate BMIm$^+$-$\mathbf{57}^-$ was prepared by ion-pair metathesis of BMIm$^+$-Cl$^-$ and K$^+$-$\mathbf{57}^-$.[87b] Surprisingly, the melting point of BMIm$^+$-$\mathbf{57}^-$ is much lower than those of the ion pairs with TMA$^+$, TEA$^+$ and TBA$^+$. Assembling behaviours of various azolium-azolate ion pairs with high phase transition temperatures were revealed by single-crystal X-ray analysis. Azolates interact with hydrogen-bonding donors, resulting in characteristic assembling modes. Ion pairs of nitroazolates with 1,3-dimethylimidazolium $\mathbf{54a}^+$ were prepared in metal-free conditions by the deprotonation of azoles with imidazolium bicarbonate or imidazolium carboxylate followed by decarboxylation.[87h] The ion pair of $\mathbf{54a}^+$ and nitroimidazolate $\mathbf{55}^-$ forms solid-state charge-by-charge assembly (Fig. 38a). In contrast, $\mathbf{56}^+$-$\mathbf{57}^-$ shows the stacking of identically charged species, forming a charge-segregated assembly, where the pyridinium unit of $\mathbf{56}^+$ is stacked with the pyridinium units of adjacent $\mathbf{56}^+$ (Fig. 38b).[87e] $\mathbf{56}^+$ is stacked with $\mathbf{58}^-$ on the pyridinium unit, resulting in a charge-by-charge assembly of $\mathbf{56}^+$-$\mathbf{58}^-$ (Fig. 38c). The anion unit in $\mathbf{54a}^+$-$\mathbf{58}^-$ is partially stacked with identically charged species, resulting in an intermediate assembling mode (Fig. 38c).[87h]

Charge-segregated assemblies are obtained for several tetrazolate ion pairs. In $\mathbf{59}^+$-$\mathbf{61a}^-$, $\mathbf{61a}^-$ is stacked with another anion, whereas $\mathbf{59}^+$ is assembled *via* hydrogen bonding (Fig. 38d(i)).[87g] In the crystal structure of $\mathbf{60a}^+$-$\mathbf{61a}^-$, the tetrazole unit of the anion is stacked with the nitro group of the adjacent anion as well as the cation, resulting in a partially charge-segregated structure (Fig. 38d(i)).[87c]

The ion pairs of a tetrazolate dimer $\mathbf{62a}^{2-}$ were synthesized using ion-pair metathesis of triazolium iodide with Ag_2SO_4, followed by another metathesis with a Ba^{2+} salt of a tetrazolate dimer.[87d,g] The resulting $2\mathbf{59}^+$-$\mathbf{62a}^{2-}$ ion pair shows $\mathbf{59}^+$ located beside $\mathbf{62a}^{2-}$ owing to the presence of hydrogen bonding between the amino group of $\mathbf{59}^+$ and a tetrazole N of $\mathbf{62a}^{2-}$ (Fig. 38d(ii)). In addition, $\mathbf{62a}^{2-}$ is slip-stacked with adjacent $\mathbf{62a}^{2-}$, giving a tilted anionic columnar structure.[87g] Conversely, in the crystal structure of $2\mathbf{60b}^+$-$\mathbf{62a}^{2-}$, two $\mathbf{60b}^+$ units are located at both sides of the diazo group of $\mathbf{62a}^{2-}$ (Fig. 38d(ii)).[87d] The ion pair comprising $\mathbf{60b}^+$ and $\mathbf{62a}^{2-}$ forms a columnar structure as they are stacked alternately in a short interplanar distance of 3.04 Å. In the case of $\mathbf{54b}^+$-$\mathbf{61b}^-$, $\mathbf{61b}^-$ arranged at the side of adjacent $\mathbf{61b}^-$ through hydrogen-bonding interaction results in a belt-like structure of $\mathbf{61b}^-$ and a stacked structure of $\mathbf{54b}^+$ (Fig. 38d(iii)).[87f] Ion pairs $\mathbf{54a}^+$-$\mathbf{62b}^-$ and $\mathbf{54b}^+$-$\mathbf{62b}^-$ were prepared by treating bis(tetrazolyl)amine, the protonated form of $\mathbf{62b}^-$, with $AgNO_3$, followed by ion-pair metathesis with $\mathbf{54a,b}^+$-I$^-$.[87i] A single crystal of $2\mathbf{54b}^+$-$\mathbf{62b}^{2-}$ was obtained by recrystallizing $\mathbf{54b}^+$-$\mathbf{62b}^-$, the corresponding monoanionic ion pair, from the MeOH/EtOAc solution. In the crystal structures of $\mathbf{54a}^+$-$\mathbf{62b}^-$ and $2\mathbf{54b}^+$-$\mathbf{62b}^{2-}$, $\mathbf{62b}^-$ and $\mathbf{62b}^{2-}$ form hydrogen-bonding dimers, exhibiting alternate

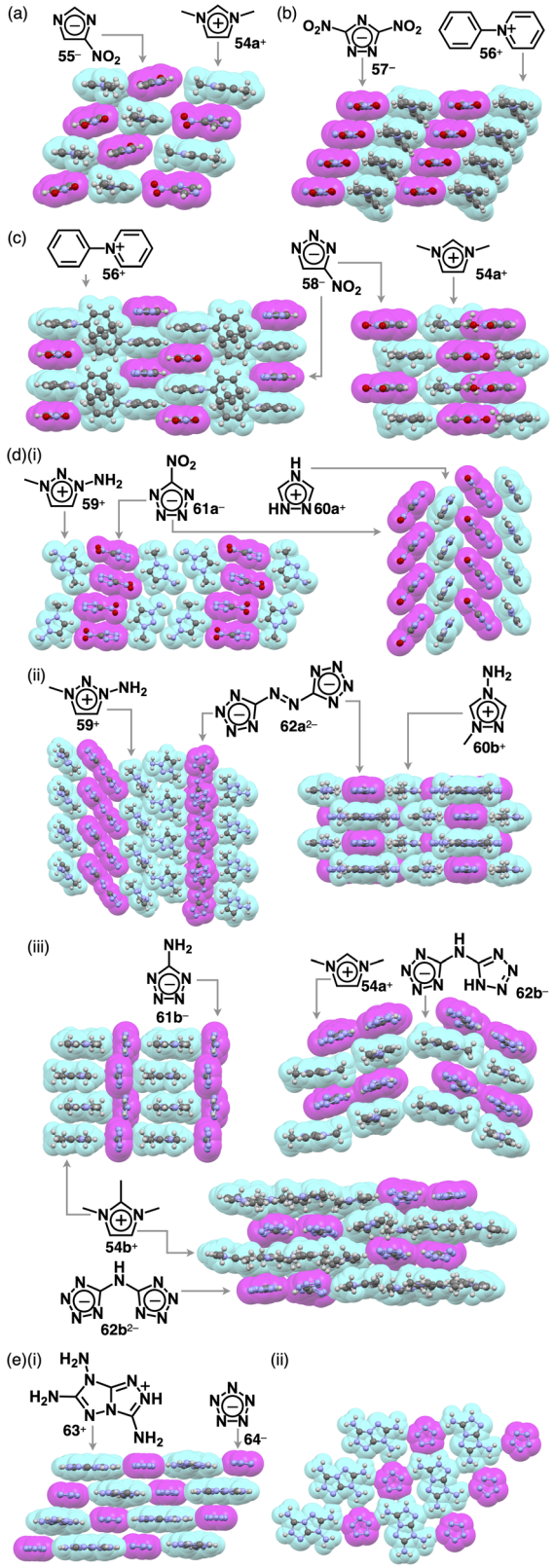

Fig. 38 Single-crystal X-ray structures of ion pairs comprising (a) imidazolate **55**$^-$, (b) 1,2,4-triazolate **57**$^-$, (c) 1,2,3-triazolate **58**$^-$, (d) tetrazolate (i) **61a**$^-$, (ii) **62a**$^{2-}$ and (iii) **61b**$^-$, **62b**$^-$ and **62b**$^{2-}$ and (e) pentazolate **64**$^-$ as (i) side and (ii) top views (redrawn from cif files: 902237, 733829, 733828, 902240, 837299, 280499, 837300, 265160, 855087, 913585, 913586 and 1973518).

stacking between the anion dimers and the coexisting two or four cation units, respectively. Additionally, in **54a**$^+$-**62b**$^-$, the **62b**$^-$ dimer is partially stacked with another dimer, while in 2**54b**$^+$-**62b**$^{2-}$, the **62b**$^{2-}$ dimer is surrounded by **54b**$^+$.[87i] Furthermore, pentazolate, cyclopentadienide analogue, with all CHs replaced by nitrogen, was also reported as π-electronic ion pairs. In **63**$^+$-**64**$^-$, all the amino groups of **63**$^+$ and nitrogen of **64**$^-$ participated in hydrogen bonding, providing a two-dimensional hydrogen-bonding network further stacked *via* ^{i}π–^{i}π interactions (Fig. 38e).[87j] Hydrogen-bonding interaction often affects the assembling modes of ion-pairing assemblies, resulting in segregated columnar structures consisting of identically charged species.

4.3. π-Electronic ion pairs comprising polymethine-based anions

Monomethine-based π-electronic anions **65**$^-$ and **66**$^{2-}$ were found to form π-electronic ion-pairing assemblies when combined with π-electronic cations (Fig. 39a).[88–90] The ion pairs of triphenyl(thio)pyryliums **67a,b**$^+$ with tetracyanoallyl anion **65**$^-$ were synthesized by ion-pair metathesis of the ClO_4^- salts of the cations with Na$^+$-**65**$^-$.[88a] In $CHCl_3$, **67a,b**$^+$-**65**$^-$ exhibits CT bands at 570 and 595 nm, respectively (Fig. 39b(i)). The CT bands exhibited negative solvatochromism, which is well-known for zwitterionic systems without electronically neutral resonance structures such as Reichardt's dyes.[91] The difference in the redox potentials of the cations correlates with the

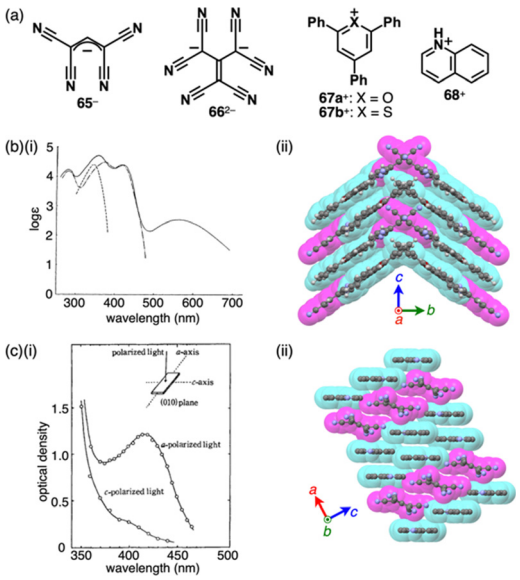

Fig. 39 Monomethine-based cyanocarbon anions and the countercations, (b) (i) UV/vis absorption spectra of **67a**$^+$-**65**$^-$ (solid line), **67a**$^+$-ClO_4^- (chain line) and Na$^+$-**65**$^-$ (dashed line) in $CHCl_3$ (redrawn from ref. 88a. Copyright 1970 CSJ) and (ii) single-crystal X-ray structure of **67a**$^+$-**65**$^-$ and (c) (i) polarized absorption spectra of 2**68**$^+$-**66**$^{2-}$ along with the direction of the long and short axes (redrawn from ref. 89a. Copyright 1969 CSJ) and (ii) single-crystal X-ray structure of 2**68**$^+$-**66**$^{2-}$. The long axes of single crystals of **67a**$^+$-**65**$^-$ and 2**68**$^+$-**66**$^{2-}$ corresponded to the *c* and *a* axes in (ii), respectively. The crystal structures are redrawn from cif files: 1240563 and 1245498.

excitation energies of the CT bands. Variable-concentration UV/vis absorption spectra afford association constants of $\sim 10^4$ and $\sim 10^5$ M^{-1} for **67a**$^+$-**65**$^-$ and **67b**$^+$-**65**$^-$, respectively.[88a] In the **67a**$^+$-**65**$^-$ ion pair, **67a**$^+$ is stacked with another **67a**$^+$ on the pyrylium core and a phenyl group in an antiparallel arrangement, resulting in a stacked dimer, which is further stacked with **65**$^-$ on both faces (Fig. 39b(ii)).[88d] This configuration leads to an intensified CT band in the polarized absorption spectrum of **67a**$^+$-**65**$^-$ aligned with the crystal growth direction, corresponding to the stacking direction (*c* axis in Fig. 39b(ii)).[88a] In contrast, the ion pair **67b**$^+$-**65**$^-$ exhibits the CT fluorescence at 740 nm in the crystalline state, while it shows no CT fluorescence in solution (measured up to ~800 nm), emitting light from the monomeric form of **67b**$^+$.[88b] Interestingly, in a frozen polar solvent (MeOH-EtOH (1 : 1)), its spectral feature is similar to that of **67b**$^+$-ClO_4^-, whereas in a frozen low polar solvent (2-methyl-THF-toluene (9 : 1)), CT fluorescence is observed at 585 nm.[88b] The photoconductivity of **67b**$^+$-**65**$^-$ is much larger than that of **67b**$^+$-ClO_4^- owing to the interionic CT absorption.[88c] **67b**$^+$-**65**$^-$ exhibits weak ESR signals even under dark conditions, whereas **67b**$^+$-ClO_4^- is ESR silent. The ESR signal intensity of **67b**$^+$-**65**$^-$ under photoirradiation is decreased upon cooling. The carrier mobility μ of **67b**$^+$-**65**$^-$ was estimated to be 10^{-5}–10^{-6} cm^2 V^{-1} s^{-1}, assuming that the carrier concentration under dark conditions was similar to the spin concentration determined by ESR.[88c]

π-Electronic ion pair of hexacyanotrimethylenemethandiide **66**$^{2-}$ with quinolinium **68**$^+$ exhibits a broad absorption band in $CHCl_3$/EtOH (Fig. 39c(i)).[89a] Moreover, the ion pairs with pyridinium and *N*-methylacridinium cations display CT absorption bands that are red-shifted according to the increased electron affinity of the cations. In **268**$^+$-**66**$^{2-}$, two cations are located in the antiparallel orientation with an interplanar distance of 3.68 Å. The stacked cation dimer and one dianion are arranged alternately with a short N···N distance of 2.99 Å, forming a two-by-one columnar structure.[89b] Similar absorption band is observed in the polarized absorption spectrum of the single crystal, indicating CT complexation (Fig. 39c(ii)).

4,4′-Bipyridines with different alkyl chains (**70**$^{2+}$, n = 1–8) were used to form ion pairs with **69**$^-$ (Fig. 40a).[90a] When shorter alkyl chains (n = 1–5) are present in the **70**$^{2+}$ ion pairs, the solid-state properties vary depending on alkyl chain lengths, as indicated by differences in melting points, XRD spacing and the intensity of CT-like absorption bands. These observations strongly suggest the formation of CT complexes in these ion pairs. Additionally, in the crystal structures of **71**–**73**$^+$-**69**$^-$, the anion **69**$^-$ is stacked by itself, giving charge-segregated assemblies (Fig. 40b).[90b] Particularly, the stacking direction in **73**$^+$-**69**$^-$ is almost perpendicular to the mean plane of the constituent charged π-systems (Fig. 40b(iii)).

π-Electronic ion pairs of further extended oppositely charged polymethines **74**–**76**$^-$ and **77**–**80**$^+$ were investigated for the effects on the spectral and assembling features (Fig. 41a).[92–94] Tatikolov *et al.* prepared the ion pairs of oppositely charged polymethine dyes. The absorption spectrum of **77**$^+$-**74a**$^-$ in

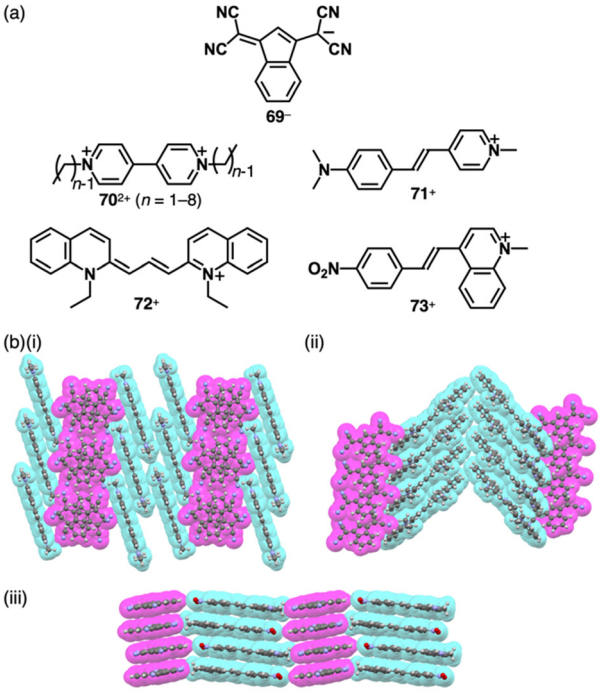

Fig. 40 (a) Polymethine-based charged π-electronic systems for ion pairs **70**$^{2+}$-**269**$^-$ and **71**–**73**$^+$-**69**$^-$ and (b) single-crystal X-ray structures of (i) **71**$^+$-**69**$^-$, (ii) **72**$^+$-**69**$^-$ and (iii) **73**$^+$-**69**$^-$ (redrawn from cif files: 1935496, 1935498 and 1935501).

CH_2Cl_2 is almost identical to the summed spectra of **77**$^+$-Br^- and TBA^+-**74a**$^-$.[92] Similarly, the absorption maxima of **78b**$^+$-**75b**$^-$ are similar to those of the components.[93] In contrast, **78a**$^+$-**75a**$^-$, whose components show overlapped absorptions in toluene at ~560–580 nm, exhibits a characteristic absorption band at ~520 nm, indicating interchromophoric interactions (Fig. 41b). Theoretical calculations supported the notably blue-shifted absorption bands of **78a**$^+$-**75a**$^-$, while showing negligible changes in the case of **78b**$^+$-**75b**$^-$.[93] Photovoltaic cell based on **77**$^+$-**74a**$^-$ shows significantly higher external quantum efficiency compared to that based on Na^+-**74a**$^-$ (Fig. 41c).[92] Focusing on assembled structures, in **79**$^+$-**76**$^-$ forming the charge-segregated assembly, **79**$^+$ and **76**$^-$ are independently stacked in brickwork-like and columnar structures, respectively (Fig. 41d(i)).[94] In contrast, the stacking of identical species is hindered in **80**$^+$-**74b**$^-$ owing to the introduction of a phenyl group at the centre of the polymethine chains, resulting in partial stacking between the oppositely charged species at their terminal π-electronic systems (Fig. 41d(ii)).

4.4. π-Electronic ion pairs comprising anions formed by deprotonation

In Sections 4.2 and 4.3, π-electronic anions that form different types of π-electronic ion pairs are discussed. These anions are obtained through deprotonation of the corresponding π-electronic systems. Similarly, π-electronic dianions can be prepared by removing protons attached to the π-electronic systems, resulting in the formation of ion pairs and assemblies. By employing ion-pair metathesis between three different deprotonated anions (eosine 2Na^+-**81a**$^{2-}$, erythrosine 2Na^+-**81b**$^{2-}$ and

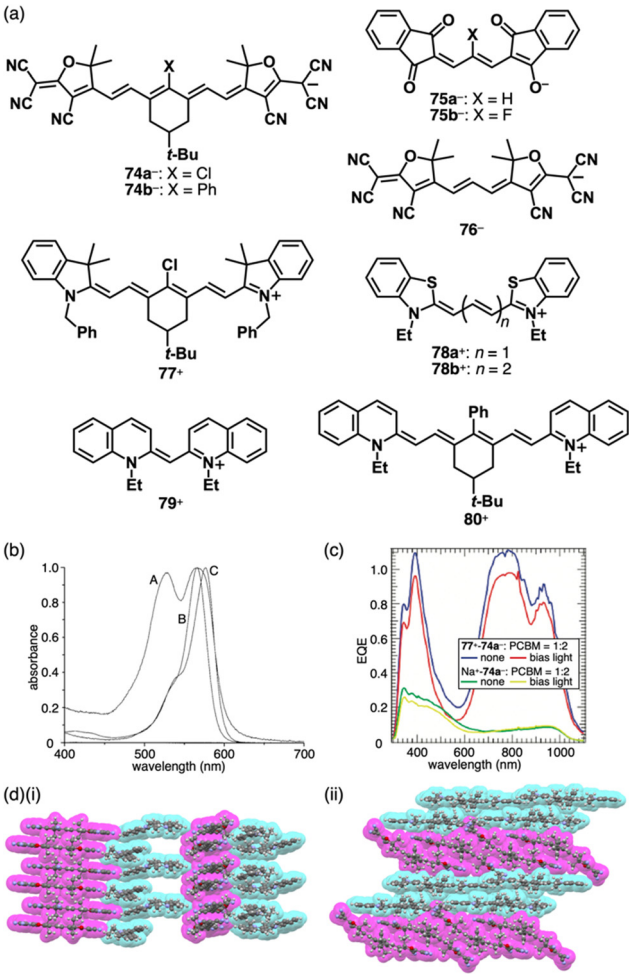

Fig. 41 (a) Extended polymethine-based π-electronic anions **74**–**76**$^-$ and the countercations **77**–**80**$^+$, (b) UV/vis absorption spectra of **78a**$^+$-**75a**$^-$ (A), 1,3-bis(dimethylamino)propenium-**75a**$^-$ (B) and **78a**$^+$-I$^-$ (C) in toluene (redrawn from ref. 93. Copyright 2001 ACS), (c) external quantum efficiency (EQE) of bulk heterojunction solar cells fabricated with ion pairs **77**$^+$-**74a**$^-$ (blue, red) and Na$^+$-**74a**$^-$ (green, yellow) blended with [60]PCBM in a 2 : 1 weight ratio (for comparison, the EQE spectra measured with and without white light bias are shown) (redrawn from ref. 92. Copyright 2009 ACS) and (d) single-crystal X-ray structures of (i) **79**$^+$-**76**$^-$ and (ii) **80**$^+$-**74b**$^-$ (redrawn from cif files: 1910541 and 1910529).

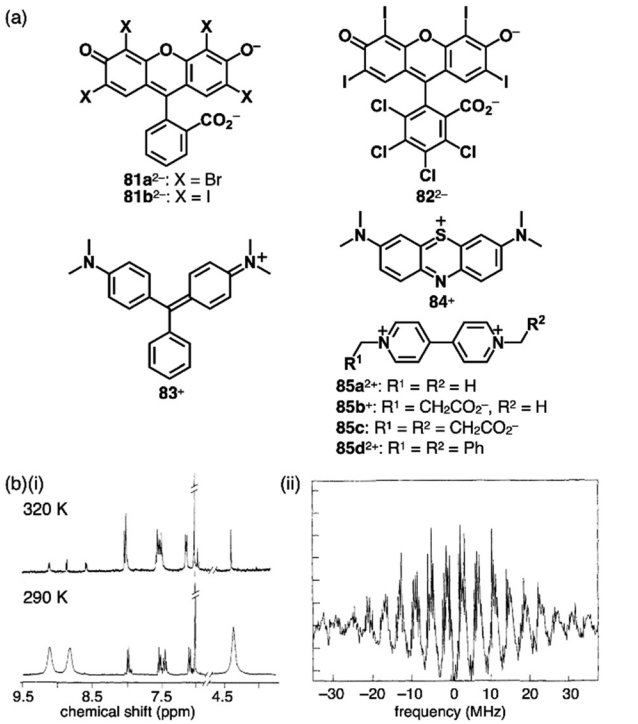

Fig. 42 (a) Xanthene-based π-electronic anions **81a,b**$^{2-}$ and **82**$^{2-}$, the countercations **83,84**$^+$, **85a,d**$^{2+}$ and **85b**$^+$ and neutral **85c** and (b) (i) ^{1}H NMR and (ii) ESR spectra of **85a**$^{2+}$-**81a**$^{2-}$ in DMSO-d_6 at 320 and 290 K and in DMSO at 295 K, respectively (redrawn from ref. 96c. Copyright 1992 ACS).

rose bengal 2Na$^+$-**82**$^{2-}$) and three different cations (crystal violet **2**$^+$-Cl$^-$ (Section 2.1), malachite green **83**$^+$-Cl$^-$ and methylene blue **84**$^+$-Cl$^-$) in aqueous solutions (Fig. 42a), nine types of π-electronic ion pairs (**22**$^+$-**81a**$^{2-}$, **22**$^+$-**81b**$^{2-}$, **22**$^+$-**82**$^{2-}$, **283**$^+$-**81a**$^{2-}$, **283**$^+$-**81b**$^{2-}$, **283**$^+$-**82**$^{2-}$, **284**$^+$-**81a**$^{2-}$, **284**$^+$-**81b**$^{2-}$ and **284**$^+$-**82**$^{2-}$) were obtained.[95] These ion pairs exhibit distinct electrical resistivity at 20 °C in compressed disk states, with resistivity values ranging from 2.5 × 10^9 Ω cm for **284**$^+$-**81a**$^{2-}$ to 3.1 × 10^{14} Ω cm for **283**$^+$-**82**$^{2-}$.

Ion-pairing behaviours in aqueous solutions were investigated by water-soluble charged π-electronic systems such as **81a**$^{2-}$.[96] Anionic fluorescence dyes in diluted aqueous solutions show fluorescence quenching by adding π-electronic cations.[96a] The absorption spectra of mixed solutions comprising different dyes such as 2Na$^+$-**81a**$^{2-}$ and **2**$^+$-Cl$^-$ are different from the sum of those of the components, suggesting the ion pairing in aqueous solution. Fluorescence quantum yields of the ion pairs in organic solvents are considerably lower than those in aqueous solution.[96a] In particular, a new absorption band appears upon increasing the concentration of 2Na$^+$-**82**$^{2-}$ in an aqueous solution containing **85a**$^{2+}$-2Cl$^-$ (~10^{-5} M) (Fig. 42a).[96b] Variable concentration measurements revealed an association constant of 9000 M^{-1} at 298 K. In addition, similar measurements for the methylviologen derivatives whose charges are partially compensated by negatively charged substituents, **85b**$^+$ and **85c**, suggest that the contributions of electrostatic attractions to the enthalpy changes are −1.1 to −1.3 kcal mol^{-1} in aqueous solutions.

In the crystal structure of **85a**$^{2+}$-**81a**$^{2-}$, **81a**$^{2-}$ is stacked with **85a**$^{2+}$ in the interplanar distance of 3.43 Å.[96c] The resulting *π-sip* forms a slip-stacked arrangement with another *π-sip* through contact between the xanthene units of two **81a**$^{2-}$ units that are arranged in the antiparallel orientation. The stacked tetrad is slip-stacked with another tetrad using the remaining part of the xanthene unit of **81a**$^{2-}$, resulting in the formation of a columnar structure. In **85d**$^{2+}$-**81a**$^{2-}$, the dianion **81a**$^{2-}$ is stacked with another **81a**$^{2-}$ in the interplanar distance of 3.76 Å in an antiparallel fashion. The stacked dianion dimer and one dication are alternately stacked with an interplanar distance of 3.58 Å, while another dication is positioned between the columns comprising one dication and two dianion. For **85a**$^{2+}$-**81a**$^{2-}$, partial dissociation is observed in DMF with an

association constant of 91 000 M^{-1}. In this solvent, the stacked ion pair is further converted to **85a**$^{2+}$-[**81a**$^{2-}$-**85a**$^{2+}$-**81a**$^{2-}$]. Intriguingly, the ^{1}H NMR signals assigned to **85a**$^{2+}$ of **85a**$^{2+}$-**81a**$^{2-}$ in DMSO-d_6 broaden upon increasing temperature and disappear at 320 K, and the ESR is observed in DMSO at 295 K, indicating the presence of a thermally accessible CT state **85a**$^{\bullet+}$-**81a**$^{\bullet-}$ (Fig. 42b).[96c]

Deprotonated dipyrrolylnitrophenols **34a,b**$^-$ (Fig. 21a) were used for the components of π-electronic ion-pairing assemblies.[67c] π-Electronic cations, ^{3}TATA$^+$ and **22a**$^+$, and π-electronic anions, **34a,b**$^-$, are alternately stacked with the stacking distances in the range of 3.27–3.47 Å, forming charge-by-charge assemblies (Fig. 43a and b).[67c] **35a**$^-$ exhibits charge-by-charge assemblies with ^{3}TATA$^+$ and **22d**$^+$ in the solid state (Fig. 43c).[68]

As described in Section 2.3, quinone methide units effectively stabilize π-electronic anions.[69] In addition, as represented by Yang's diradical,[97] combinations of multiple quinone methide units can provide open-shell species, whose spin states depend on the bridging unit as spin coupler; however, the ground state of **36**$^-$ is closed-shell state.[69] Modifications of the deprotonated pyrrole-based quinoidal systems induce remarkable electronic properties derived from the molecular structures and interactions with coexisting cations. Quinoidal systems exhibit unique diradical properties, with their singlet and triplet states dependent on the linker units acting as spin couplers. The PB core, which has been employed for anion binding (Section 3), possesses a partially cross-conjugated structure that functions as a singlet coupler, resembling a polarized carbonyl unit (Fig. 44a). PB-based quinone methide **86** (Fig. 44b(i)), which is an oxidized form of PB, was synthesized as a benzo-fused derivative to enhance stability.[98] **86** was deprotonated by TBAOH and NaOH to provide **86**$^-$ in the forms of TBA$^+$ and Na$^+$ ion pairs, the latter of which was further converted to a ^{3}TATA$^+$ ion pair by ion-pair metathesis (Fig. 44b(i)). In the crystal structure of ^{3}TATA$^+$-**86**$^-$, ^{3}TATA$^+$ and **86**$^-$ are alternately stacked with their π-systems, creating the charge-by-charge assembly (Fig. 44b(ii)). Upon further deprotonation of the ion pairs of **86**$^-$ with TBA$^+$ and ^{3}TATA$^+$ by TBAOH, the dianion **86**$^{2-}$ was formed, resulting in the ion pairs 2TBA$^+$-**86**$^{2-}$ and ^{3}TATA$^+$-TBA$^+$-**86**$^{2-}$, respectively (Fig. 44c). Unlike **86** and the

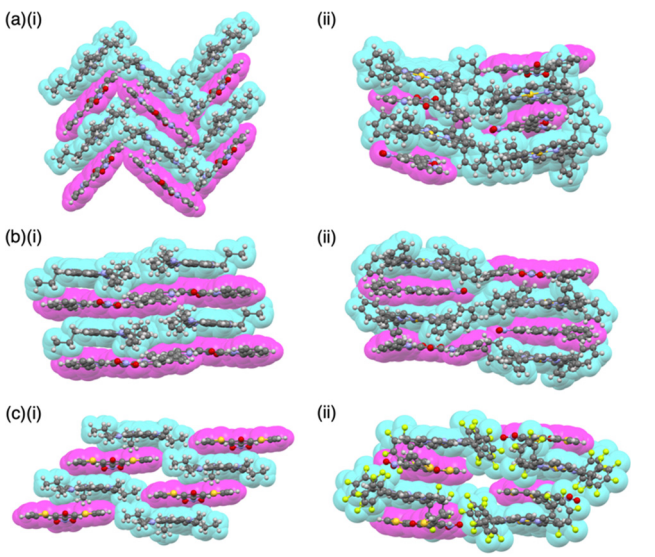

Fig. 43 Single-crystal X-ray structures of diarylnitrophenoxides: (a) (i) ^{3}TATA$^+$-**34a**$^-$ and (ii) **22a**$^+$-**34a**$^-$, (b) (i) ^{3}TATA$^+$-**34b**$^-$ and (ii) **22a**$^+$-**34b**$^-$ and (c) (i) ^{3}TATA$^+$-**35a**$^-$ and (ii) **22d**$^+$-**35a**$^-$(redrawn from cif files: 2061520, 2061524, 2061521, 2061525, 2253152 and 2253153).

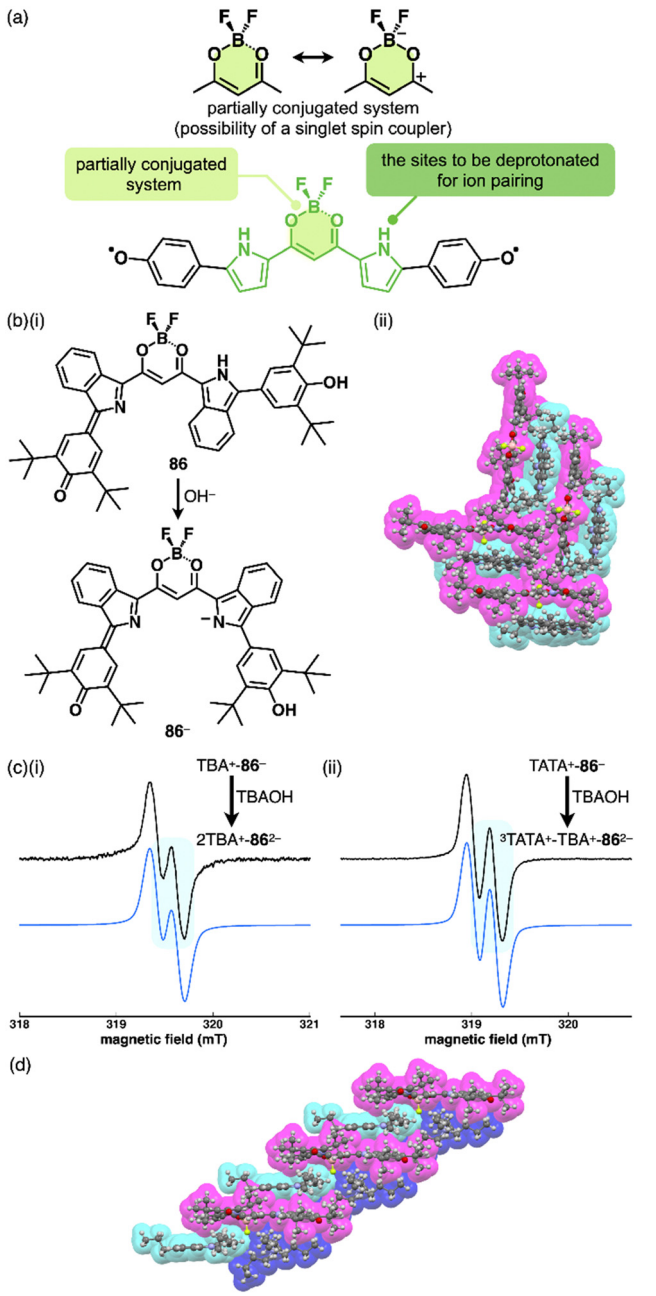

Fig. 44 (a) Resonance structures of diketone-boron complex (top) and conceptual diagram of PB-based quinoidal molecule represented in the diradical tautomer of the parent form (bottom), (b) (i) formation of quinoidal dipyrrolyldiketone boron complex in the form of monoanion **86**$^-$ by deprotonation of **86** and (ii) single-crystal X-ray structure of ^{3}TATA$^+$-**86**$^-$, (c) ESR spectra of (i) 2TBA$^+$-**86**$^{2-}$ and (ii) ^{3}TATA$^+$-TBA$^+$-**86**$^{2-}$ in mesitylene (1 mM) (black line) and corresponding simulation patterns (blue line) and (d) single-crystal X-ray structure of ^{3}TATA$^+$-TBA$^+$-**86**$^{2-}$ (redrawn from ref. 98. Copyright 2023 ACS). The crystal structures are redrawn from cif files: 2225435 and 2225436.

monoanion **86**$^{-}$, the dianion **86**$^{2-}$ in 2TBA^{+}-**86**$^{2-}$ exhibits sharp and broad ^{1}H NMR signals at −50 °C and r.t., respectively, in CD_2Cl_2 and displays the ESR signals with a *g* value of 2.003 at r.t. in mesitylene (Fig. 44c(i)). These observations indicate a ground-state singlet diradical character. Additionally, the ESR signals of ^{3}TATA^{+}-TBA^{+}-**86**$^{2-}$ differ from those of 2TBA^{+}-**86**$^{2-}$, displaying countercation-dependent magnetic properties (Fig. 44c(ii)). The ground-state singlet diradical nature is further confirmed by the enhancement of the variable-temperature ESR for ^{3}TATA^{+}-TBA^{+}-**86**$^{2-}$, yielding an estimated ΔE_{ST} of −6.4 kcal mol^{-1}. The interaction between **86**$^{2-}$ and ^{3}TATA^{+} is also observed in single-crystal X-ray analysis of ^{3}TATA^{+}-TBA^{+}-**86**$^{2-}$, wherein TBA^{+} is situated on the PB unit of **86**$^{2-}$ with reduced contact of ^{3}TATA^{+} and **86**$^{2-}$ (Fig. 44d).[98]

Moreover, deprotonated hydroxyporphyrins are also adopted in π-electronic ion pairs. Assembling behaviours of ^{3}TATA^{+} ion pairs of anionic porphyrin free base **37**$^{-}$ and Ni^{II} and Pd^{II} complexes **37a,c**$^{-}$ were investigated (Fig. 45a).[9] The anions are stacked with ^{3}TATA^{+} to form charge-by-charge assemblies in the crystal structures. In ^{3}TATA^{+}-**37a**$^{-}$, each component is stacked with identically charged species, resulting in a partially charge-segregated mode (Fig. 45b). The absorption spectrum of ^{3}TATA^{+}-**37a**$^{-}$ in the solid state exhibits blue-shifted and red-shifted bands derived from **37a**$^{-}$ and ^{3}TATA^{+}, respectively, compared to those for the monomeric states of **37a**$^{-}$ (TBA^{+}-**37a**$^{-}$) and ^{3}TATA^{+} (^{3}TATA^{+}-Cl^{-}) in CH_2Cl_2 (Fig. 45c). This shift is attributed to exciton coupling arising from the stacking of identically charged species in the parallel (H-like) arrangement for **37a**$^{-}$ and a head-to-tail (J-like) arrangement for ^{3}TATA^{+}. Additionally, solid-state transient absorption spectra of ^{3}TATA^{+}-**37a**$^{-}$ reveal the generation of radical **37a**$^{\bullet}$ by the PET between the π-electronic systems. Furthermore, EDA of the packing structure of ^{3}TATA^{+}-**37a**$^{-}$ indicates a significant contribution of electrostatic and dispersion forces in stabilizing the stacked structures of the constituent π-electronic ions.[9]

Remarkable electronic properties emerge from π-electronic ion pairs and their assemblies comprising charged species with large π-systems. Promising π-electronic ion pairs can be produced by introducing charged porphyrins as cations and anions, including **37a**$^{-}$ for the latter. Modifications of the electronic states and resulting assembled structures can be achieved by introducing substituents, as seen in Au^{III} complexes **22a,c**$^{+}$ that possess four C_6H_5 and C_6F_5 moieties, respectively, at the *meso* positions.[52] Combining oppositely charged porphyrins with distinct electronic states according to introduced substituents provides diverse ion pairs that can be used for functional materials. Thus, in addition to **37a**$^{-}$, *meso*-phenyl-substituted **87**$^{-}$ was prepared as an electron-rich "activated" anion (Fig. 46a).[6] The "activated" cation **22d**$^{+}$, with three *meso*-C_6F_5 units for efficient stacking, has been a focal point for creating an activated ion pair with **87**$^{-}$. Several porphyrin ion pairs, including **22a**$^{+}$-**37a**$^{-}$,[52a] **22a**$^{+}$-**87**$^{-}$ and **22d**$^{+}$-**37a**$^{-}$ as well as the activated ion pair **22d**$^{+}$-**87**$^{-}$, were prepared by ion-pair metathesis from charged porphyrin starting

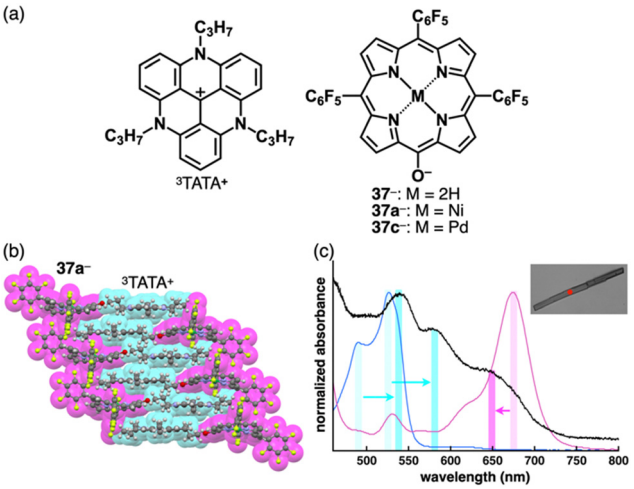

Fig. 45 (a) Ion pairs ^{3}TATA^{+}-**37**$^{-}$ and ^{3}TATA^{+}-**37a,c**$^{-}$, (b) single-crystal X-ray structure of ^{3}TATA^{+}-**37a**$^{-}$ (redrawn from a cif file: 1906678) and (c) UV/vis absorption spectrum of the single crystal of ^{3}TATA^{+}-**37a**$^{-}$ (black) along with those of the solution states (1 × 10^{-5} M in CH_2Cl_2) of TBA^{+}-**37a**$^{-}$ (magenta) and ^{3}TATA^{+}-Cl^{-} (cyan) (inset: optical microscopy image of a single crystal of ^{3}TATA^{+}-**37a**$^{-}$) (redrawn from ref. 9. Copyright 2021 RSC).

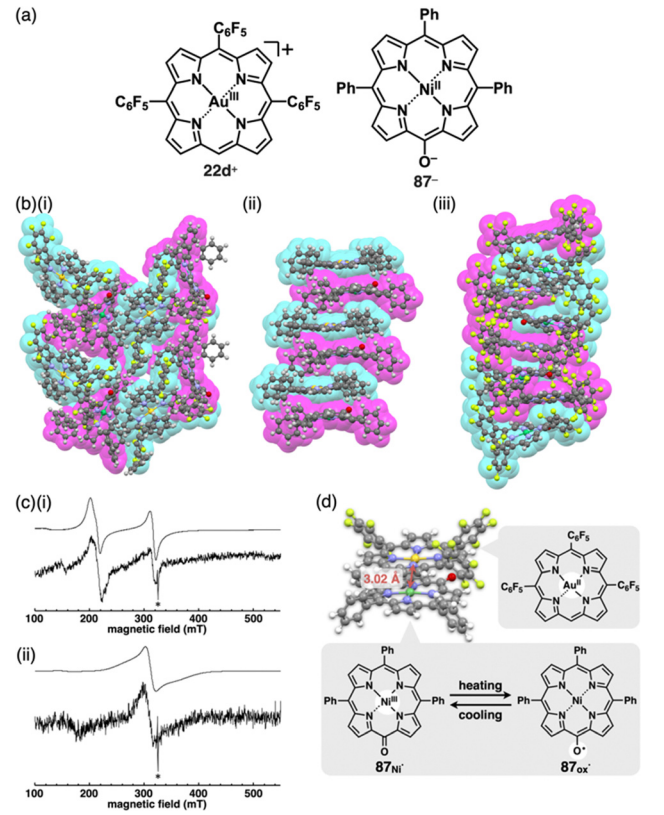

Fig. 46 (a) Ion pair of charged porphyrins, **22d**$^{+}$-**87**$^{-}$, as an activated ion pair, (b) single-crystal X-ray structures of (i) **22d**$^{+}$-**87**$^{-}$, (ii) **22a**$^{+}$-**87**$^{-}$ and (iii) **22d**$^{+}$-**37a**$^{-}$ (redrawn from cif files: 2201074, 2201075 and 2201076), (c) simulated (top) and observed (bottom) ESR spectra of **22d**$^{+}$-**87**$^{-}$ in toluene at (i) 10 and (ii) 140 K and (d) closely stacked structure (*π-srp*) of **22d**$^{\bullet}$ and **87**$^{\bullet}$ with the spin–spin distance and the change in spin distribution of **87**$^{\bullet}$ (**87**$_{Ni}^{\bullet}$ and **87**$_{ox}^{\bullet}$) as a result of temperature change (redrawn from ref. 6. Copyright 2022 ACS). Signals marked with * in (c) are ascribable to a trace amount of dissociated **87**$^{\bullet}$, whereas white circles in (d) represent spin distributions.

materials, resulting in solid-state ion-pairing assemblies. In the case of **22a**$^+$-**37a**$^-$, stacking arrangement exhibits a zigzag pattern owing to the steric effect of *meso*-phenyl groups.[52a] In contrast, the assembly of **22d**$^+$-**87**$^-$ involves a charge-segregated mode, with four benzene molecules included for each ion pair (Fig. 46b(i)). Nevertheless, *π-sip*-based charge-by-charge assembly modes in **22a**$^+$-**87**$^-$ results in $^i\pi$–$^i\pi$ interaction between porphyrin ions, as the steric hindrance of the porphyrin anion is relaxed (Fig. 46b(ii)). The packing diagram in **22d**$^+$-**37a**$^-$ demonstrates a 1D-chain structure of *π-sip* assembled in a four-fold helical symmetry, with **22d**$^+$ and **37a**$^-$ arranged in a stacking distance of 3.57 Å (Fig. 46b(iii)).[6,99]

Charged porphyrins form stacked dimers in solution, as detected by ^{1}H NMR chemical shifts derived from shielding and deshielding effects. Concentration-dependent ^{1}H NMR of **22d**$^+$-**37a**$^-$ in CD_2Cl_2 provides the heterodimerization constant ($K_{dim} = 2.8 \times 10^5$ M^{-1}) at 20 °C. On the other hand, the UV/vis absorption spectrum of **22d**$^+$-**37a**$^-$ in the *π-sip* is almost the sum of the spectra of constituent **22d**$^+$ and **37a**$^-$. In contrast, the activated ion pair **22d**$^+$-**87**$^-$ exhibits a UV/vis absorption spectrum that differs from the corresponding summed spectra in less polar solvents. The spectrum observed in toluene is consistent with the combined spectra of the reduced Au^{II} complex **22d**$^\bullet$ and the oxidized Ni^{II} complex oxyradical **87**$_{ox}^\bullet$, indicating an electron transfer from **87**$^-$ to **22d**$^+$ to generate a π-stacked radical pair (*π-srp*). Notably, the ESR spectrum in frozen toluene at 10 K (Fig. 46c(i)) displays the *π-srp* as a pair of **22d**$^\bullet$ and Ni^{III} complex **87**$^\bullet$ with a short spin–spin distance of 3.02 Å (Fig. 46d top). VT ESR spectra suggest spin transfer in **87**$^\bullet$ and antiferromagnetic interaction in *π-srp* (Fig. 46c(ii) and d bottom).[6] The less activated porphyrin ion pairs exhibit *π-sips* that correlate with the redox potentials of their constituent components based on the substituents. Further investigations on the PET for ion pairs, including triaryl-substituted **22b**$^+$ and **22d**$^+$, revealed varying electron-transfer rates, leading to the formation of excited-state radical species. These findings suggest application potential of these ion pairs in photocatalysis owing to their tuneable electronic state.[6,53]

5. Conclusions

π-Electronic ion pairs, comprising countercharged π-electronic systems, hold immense potential in generating structured assembled arrangements and displaying unique properties. Assembling modes of charged components are modulated by their geometries and electronic states. Thus, the design and synthesis of charged π-electronic systems are crucial for the fabrication of ion-pairing assemblies (Fig. 47). The presence of charges within the core π-electronic units makes their preparation challenging owing to the inherent reactivity arising from electron-deficient and -rich states. Furthermore, the specific combinations of π-electronic ions are crucial for determining the nature of the assemblies and the resulting properties. Less stable π-electronic ions can be stabilized by combining specific counterions *via* the formation of *π-sips* based on $^i\pi$–$^i\pi$ interactions. Hence, diversity is a central aspect in ion-pairing chemistry.

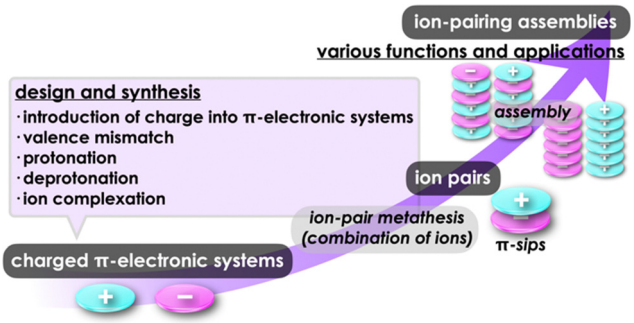

Fig. 47 Formation of ion-pairing assemblies through design and synthesis of charged π-electronic systems, ion-pair metathesis and assembly.

The assemblies of ion pairs reveal their distinct characteristics not only in solution but also in bulk states like crystals and soft materials. The ability to control assembling modes, whether charge-by-charge or charge-segregated, is crucial for exhibiting specific electronic properties based on the arrangements. The electronic properties of π-electronic ion pairs and their assemblies are distinct from those of electronically neutral π-systems. The proximally located oppositely charged π-electronic systems induce the polarized columnar structures, most polarizations of which are cancelled by those of neighbouring columns. Spontaneous polarization with uniform alignment of polarized columns facilitates the development of ferroelectric materials.[100] The manipulation of redox potentials between π-electronic cations and anions enables electron transfer in both excited and ground states. The resulting radical pairs, especially under photoirradiation, can serve as catalysts, with cation- and anion-derived radicals acting as reducing and oxidizing species, respectively.[101] Furthermore, columnar structures comprising identically charged species offer potential applications in efficient semiconductive materials. The electrostatic repulsion between identically charged species can be overcome by dispersion forces originating from π-electronic systems and dipole–dipole interactions in polarized charged species. These strategies are easily attainable through simple modifications for π-electronic systems, in contrast to inorganic ionic species. This review article showcases the production of diverse π-electronic ion pairs, demonstrating possibilities for future property investigations and applications. The authors have made significant strides in understanding their intriguing behaviours of these ion pairs through thorough comprehensive studies in synthesis, combination, assembly and electronic and photophysical properties in recent years.[102] A significant portion of ion-pairing chemistry remains unexplored and awaits exploration through ongoing research endeavours.

Conflicts of interest

There are no conflicts of interest to declare.

Acknowledgements

The recent contributions of our group reported herein were mainly supported by JSPS KAKENHI Grant Numbers JP18H01968 and JP22H02067 for Scientific Research (B), JP20H05863 for Transformative Research Areas (A) "Condensed Conjugation" and the Ritsumeikan Global Innovation Research Organization (R-GIRO) project, 2017–2022 and 2022–2027.

Notes and references

1 Selected books on supramolecular assemblies for electronic materials: (*a*) *Supramolecular Soft Matter: Applications in Materials and Organic Electronics*, ed. T. Nakanishi, Wiley, 2011; (*b*) *Functional Supramolecular Architectures*, ed. P. Samorì and F. Cacialli, Wiley, 2011; (*c*) *Unimolecular and Supramolecular Electronics I: Chemistry and Physics Meet at Metal-Molecule Interfaces, Topics in Current Chemistry*, ed. R. M. Metzger, Springer, 2012; (*d*) *Supramolecular Materials for Opto-Electronics*, ed. N. Koch, RSC, 2015.

2 (*a*) K. Müller-Dethlefs and P. Hobza, *Chem. Rev.*, 2000, **100**, 143; (*b*) A. S. Mahadevi and G. N. Sastry, *Chem. Rev.*, 2016, **116**, 2775.

3 A. J. Stone, *The Theory of Intermolecular Forces*, Oxford University Press, 2013.

4 (*a*) C. F. J. Faul and M. Antonietti, *Adv. Mater.*, 2003, **15**, 673; (*b*) C. F. J. Faul, *Acc. Chem. Res.*, 2014, **47**, 3428.

5 (*a*) Y. Haketa and H. Maeda, *Bull. Chem. Soc. Jpn.*, 2018, **91**, 420; (*b*) Y. Haketa, K. Urakawa and H. Maeda, *Mol. Syst. Des. Eng.*, 2020, **5**, 757; (*c*) K. Yamasumi and H. Maeda, *Bull. Chem. Soc. Jpn.*, 2021, **94**, 2252.

6 H. Tanaka, Y. Kobayashi, K. Furukawa, Y. Okayasu, S. Akine, N. Yasuda and H. Maeda, *J. Am. Chem. Soc.*, 2022, **144**, 21710.

7 Y. Haketa, S. Sasaki, N. Ohta, H. Masunaga, H. Ogawa, N. Mizuno, F. Araoka, H. Takezoe and H. Maeda, *Angew. Chem., Int. Ed.*, 2010, **49**, 10079.

8 Several π-electronic ion-pairing assemblies had been reported as listed in the following references (*e.g.*, ref. 81*d*,*e*,82,87*c*–*e*,88*d*,89*b*,96*c*) before the report of ref. 7. However, to the best of our knowledge, no reports clearly have shown the chemistry of π-electronic ion-pairing assemblies.

9 Y. Sasano, H. Tanaka, Y. Haketa, Y. Kobayashi, Y. Ishibashi, T. Morimoto, R. Sato, Y. Shigeta, N. Yasuda, T. Asahi and H. Maeda, *Chem. Sci.*, 2021, **12**, 9645.

10 (*a*) D. F. Duxbury, *Chem. Rev.*, 1993, **93**, 381; (*b*) V. Nair, S. Thomas, S. C. Mathew and K. G. Abhilash, *Tetrahedron*, 2006, **62**, 6731.

11 E. Q. Adams and L. Rosenstein, *J. Am. Chem. Soc.*, 1914, **36**, 1452.

12 Reviews of fluorescent dyes: (*a*) R. N. Dsouza, U. Pischel and W. M. Nau, *Chem. Rev.*, 2011, **111**, 7941; (*b*) Y. Geng, Z. Wang, J. Zhou, M. Zhu, J. Liu and T. D. James, *Chem. Soc. Rev.*, 2023, **52**, 3873.

13 Reviews of rhodamines: (*a*) M. Beija, C. A. M. Afonso and J. M. G. Martinho, *Chem. Soc. Rev.*, 2009, **38**, 2410; (*b*) T. Ikeno, T. Nagano and K. Hanaoka, *Chem. – Asian J.*, 2017, **12**, 1435; (*c*) E. Reglska, P. Hindenberg and C. Romero-Nieto, *Eur. J. Inorg. Chem.*, 2019, 1519; (*d*) S. G. Keller, M. Kamiya and Y. Urano, *Molecules*, 2020, **25**, 5964.

14 Reviews and first two reports of $TATA^+$: (*a*) J. Bosson, J. Gouin and J. Lacour, *Chem. Soc. Rev.*, 2014, **43**, 2824; (*b*) A. Winter and U. S. Schubert, *Mater. Chem. Front.*, 2019, **3**, 2308; (*c*) B. W. Laursen and F. C. Krebs, *Angew. Chem., Int. Ed.*, 2000, **39**, 3432; (*d*) B. W. Laursen and F. C. Krebs, *Chem. – Eur. J.*, 2001, **7**, 1773.

15 A review and selected reports of $TOTA^+$: (*a*) A. C. Shaikh, J. M. Veleta, J. Moutet and T. L. Gianetti, *Chem. Sci.*, 2021, **12**, 4841; (*b*) B. W. Laursen, F. C. Krebs, M. F. Nielsen, K. Bechgaard, J. B. Christensen and N. Harrit, *J. Am. Chem. Soc.*, 1998, **120**, 12255; (*c*) D. Shi, C. Schwall, G. Sfintes, E. Thyrhaug, P. Hammershøj, M. Cárdenas, J. B. Simonsen and B. W. Laursen, *Chem. – Eur. J.*, 2014, **20**, 6853.

16 Examples of $TATA^+$: (*a*) R. Gueret, L. Poulard, M. Oshinowa, J. Chauvin, M. Dahmane, G. Dupeyre, P. P. Lainé, J. Fortage and M.-N. Collomb, *ACS Catal.*, 2018, **8**, 3792; (*b*) P.-Y. Ho, S.-C. Cheng, F. Yu, Y.-Y. Yeung, W.-X. Ni, C.-C. Ko, C.-F. Leung, T.-C. Lau and M. Robert, *ACS Catal.*, 2023, **13**, 5979.

17 G. Allinson, R. J. Bushby, J.-L. Paillaud and M. Thornton-Pett, *J. Chem. Soc., Perkin Trans. 1*, 1995, 385.

18 Reviews of cyanines: (*a*) A. Mishra, R. K. Behera, P. K. Behera, B. K. Mishra and G. B. Behera, *Chem. Rev.*, 2000, **100**, 1973; (*b*) M. Henary, S. Paranijpe and E. A. Owens, *Heterocycl. Commun.*, 2013, **19**, 1; (*c*) J. L. Bricks, A. D. Kachkovski, Y. L. Slominski, A. O. Gerasov and S. V. Popov, *Dyes Pigm.*, 2015, **121**, 238; (*d*) W. Sun, S. Guo, C. Hu, J. Fan and X. Peng, *Chem. Rev.*, 2016, **116**, 7768; (*e*) H. A. Shindy, *Dyes Pigm.*, 2017, **145**, 505; (*f*) K. Ilina and M. Henary, *Chem. – Eur. J.*, 2021, **27**, 4230; (*g*) H. Mustroph, *Dyes Pigm.*, 2022, **208**, 110783.

19 F. Würthner, T. E. Kaiser and C. R. Saha-Möller, *Angew. Chem., Int. Ed.*, 2011, **50**, 3376.

20 H. Mustroph, *Phys. Sci. Rev.*, 2021, **7**, 37.

21 S. Khopkar and G. Shankarling, *Dyes Pigm.*, 2019, **170**, 107645.

22 (*a*) Y. Xu, A. Malkovskiy, Q. Wang and Y. Pang, *Org. Biomol. Chem.*, 2011, **9**, 2878; (*b*) Y. Xu, A. Malkovskiy and Y. Pang, *Chem. Commun.*, 2011, **47**, 6662; (*c*) Y. Xu, B. Li, L. Xiao, J. Ouyang, S. Sun and Y. Pang, *Chem. Commun.*, 2014, **50**, 8677; (*d*) B. Li, W. Li, Y. Xu, J. Li, J. Tu and S. Sun, *Chem. Commun.*, 2015, **51**, 14652.

23 K. Yamasumi, K. Ueda, Y. Haketa, Y. Hattori, M. Suda, S. Seki, H. Sakai, T. Hasobe, R. Ikemura, Y. Imai, Y. Ishibashi, T. Asahi, K. Nakamura and H. Maeda, *Angew. Chem., Int. Ed.*, 2023, **62**, e202216013.

24 D. J. M. Lyons, R. D. Crocker, M. Blümel and T. V. Nguyen, *Angew. Chem., Int. Ed.*, 2017, **56**, 1466.

25 (*a*) K. Komatsu and T. Kitagawa, *Chem. Rev.*, 2003, **103**, 1371; (*b*) J. S. Bandar and T. H. Lambert, *Synthesis*,

2013, 2485; (*c*) R. M. Wilson and T. H. Lambert, *Acc. Chem. Res.*, 2022, **55**, 3057.
26 F. T. Zahra, A. Saeed, K. Mumtaz and F. Albericio, *Molecules*, 2023, **28**, 4095.
27 *Metallocenes: Synthesis Reactivity Applications*, ed. A. Togni and R. L. Halterman, Wiley, 1998.
28 R. Kuhn and D. Rewicki, *Angew. Chem., Int. Ed. Engl.*, 1967, **6**, 635.
29 O. Diels, *Ber. Dtsch. Chem. Ges.*, 1942, **75**, 1452.
30 M. I. Bruce, P. A. Humphrey, B. W. Skelton and A. H. White, *Aust. J. Chem.*, 1984, **37**, 2441.
31 (*a*) O. W. Webster, *J. Am. Chem. Soc.*, 1965, **87**, 1820; (*b*) T. Sakai, S. Seo, J. Matsuoka and Y. Mori, *J. Org. Chem.*, 2013, **78**, 10978.
32 A selected report: J. Bacsa, R. J. Less, H. E. Skelton, Z. Soracevic, A. Steiner, T. C. Wilson, P. T. Wood and D. S. Wright, *Angew. Chem., Int. Ed.*, 2011, **29**, 8279.
33 Y. Bando, Y. Haketa, T. Sakurai, W. Matsuda, S. Seki, H. Takaya and H. Maeda, *Chem. – Eur. J.*, 2016, **23**, 7843.
34 $PCCp^-$ as a guest species can control the states of self-assembled cage-shaped nanocubes: (*a*) Y.-Y. Zhan, T. Kojima, T. Nakamura, T. Takahashi, S. Takahashi, Y. Haketa, Y. Shoji, H. Maeda, T. Fukushima and S. Hiraoka, *Nat. Commun.*, 2018, **9**, 4530; (*b*) Y.-Y. Zhan, T. Kojima, K. Ishii, S. Takahashi, Y. Haketa, H. Maeda, S. Uchiyama and S. Hiraoka, *Nat. Commun.*, 2019, **10**, 1440.
35 (*a*) S. Sowmiah, J. M. S. S. Esperança, L. P. N. Revelo and C. A. M. Afonso, *Org. Chem. Front.*, 2018, **5**, 453; (*b*) Y. Li, H. Wang and X. Li, *Chem. Sci.*, 2020, **11**, 12249; (*c*) E. Hola and J. Ortyl, *Eur. Polym. J.*, 2021, **150**, 110365.
36 D. Wu, W. Pisula, M. C. Haberecht, X. Feng and K. Müllen, *Org. Lett.*, 2009, **11**, 5686.
37 A. Granzhan and H. Ihmels, *Synlett*, 2016, 1775.
38 (*a*) D. Wu, L. Zhi, G. J. Bodwell, G. Cui, N. Tsao and K. Müllen, *Angew. Chem., Int. Ed.*, 2007, **46**, 5417; (*b*) D. Wu, W. Pisula, V. Enkelmann, X. Feng and K. Müllen, *J. Am. Chem. Soc.*, 2009, **131**, 9620.
39 (*a*) *The Porphyrin Handbook*, ed. K. M. Kadish, K. M. Smith and R. Guilard, Academic Press, 1999; (*b*) *Handbook of Porphyrin Science*, ed. K. M. Kadish, K. M. Smith and R. Guilard, World Scientific, 2010.
40 Selected reviews: (*a*) J. A. A. W. Elemans, R. van Hameren, R. J. M. Nolte and A. E. Rowan, *Adv. Mater.*, 2006, **18**, 1251; (*b*) A. D'Urso, M. E. Fragalá and R. Purrello, *Chem. Commun.*, 2012, **48**, 8165; (*c*) H. Lee, H. Park, D. Y. Ryu and W.-D. Jang, *Chem. Soc. Rev.*, 2023, **52**, 1947.
41 A review and selected reports of heteroatom-containing porphyrins: (*a*) Y. Matano, *Chem. Rev.*, 2017, **117**, 3138; (*b*) A. Takiguchi, S. Kang, N. Fukui, D. Kim and H. Shinokubo, *Angew. Chem., Int. Ed.*, 2021, **60**, 2915; (*c*) A. Takiguchi and H. Shinokubo, *Chem. Lett.*, 2022, **51**, 590; (*d*) A. Takiguchi, N. Inai, S. Kang, M. Hagai, S. Lee, T. Yanai, D. Kim and H. Shinokubo, *Chem. Commun.*, 2022, **58**, 5956.
42 T. Satoh, M. Minoura, H. Nakano, K. Furukawa and Y. Matano, *Angew. Chem., Int. Ed.*, 2016, **55**, 2235.
43 A review and selected reports of heteroporphyrins: (*a*) T. Chatterjee, V. S. Shetti, R. Sharma and M. Ravikanth, *Chem. Rev.*, 2017, **117**, 3254; (*b*) E. Vogel, W. Haas, B. Knipp, J. Lex and H. Schmickler, *Angew. Chem., Int. Ed. Engl.*, 1988, **27**, 406; (*c*) E. Vogel, P. Röhrig, M. Sicken, B. Knipp, A. Herrmann, M. Pohl, H. Schmickler and J. Lex, *Angew. Chem., Int. Ed. Engl.*, 1989, **28**, 1651; (*d*) E. Vogel, J. Dörr, A. Herrmann, J. Lex, H. Schmickler, P. Walgenbach, J. P. Gisselbrecht and M. Gross, *Angew. Chem., Int. Ed. Engl.*, 1993, **32**, 1597; (*e*) M. Bröring, H.-J. Dietrich, J. Dörr, G. Hohlneicher, J. Lex, N. Jux, C. Pütz, M. Roeb, H. Schmickler and E. Vogel, *Angew. Chem., Int. Ed.*, 2000, **39**, 1105.
44 (*a*) G. Magnus, *Poggendorff's Ann. Phys.*, 1828, **90**, 239; (*b*) G. Magnus, *Ann. Chim. Phys.*, 1829, **40**, 110.
45 M. Atoji, J. W. Richardson and R. E. Rundle, *J. Am. Chem. Soc.*, 1957, **79**, 3017.
46 M. Fang, S. R. Wilson and K. S. Suslick, *J. Am. Chem. Soc.*, 2008, **130**, 1134.
47 Z. Xie, J. Manning, R. W. Reed, R. Mathur, P. D. W. Boyd, A. Benesi and C. A. Reed, *J. Am. Chem. Soc.*, 1996, **118**, 2922.
48 Y. Inokuma, J. H. Kwon, T. K. Ahn, M.-C. Yoo, D. Kim and A. Osuka, *Angew. Chem., Int. Ed.*, 2006, **45**, 961.
49 E. Tsurumaki, S. Y. Hayashi, F. S. Tham, C. A. Reed and A. Osuka, *J. Am. Chem. Soc.*, 2011, **133**, 11956.
50 A review of cationic Au^{III} complexes: R. Kumar and C. Nevado, *Angew. Chem., Int. Ed.*, 2017, **56**, 1994.
51 (*a*) E. B. Fleischer and A. Laszlo, *Inorg. Nucl. Chem. Lett.*, 1969, **5**, 373; (*b*) R. Timkovich and A. Tulinsky, *Inorg. Chem.*, 1977, **16**, 962; (*c*) J.-C. Chambron, V. Heitz and J.-P. Sauvage, *New J. Chem.*, 1997, **21**, 237; (*d*) H. Lv, B. Yang, J. Jing, Y. Yu, J. Zhang and J.-L. Zhang, *Dalton Trans.*, 2012, **41**, 3116.
52 (*a*) Y. Haketa, Y. Bando, Y. Sasano, H. Tanaka, N. Yasuda, I. Hisaki and H. Maeda, *iScience*, 2019, **14**, 241; (*b*) H. Tanaka, Y. Haketa, N. Yasuda and H. Maeda, *Chem. – Asian J.*, 2019, **14**, 2129.
53 H. Tanaka, Y. Okayasu, Y. Kobayashi and H. Maeda, *Chem. – Eur. J.*, 2023, **29**, e202203957.
54 L. Latos-Grażyński, J. Lisowski, M. M. Olmstead and A. L. Balch, *Inorg. Chem.*, 1989, **28**, 1183.
55 M. Fujita, H. Tanaka, N. Yasuda and H. Maeda, *Chem. Commun.*, 2022, **58**, 9870.
56 Q.-C. Chen, S. Fite, N. Fridman, B. Tumanskii, A. Mahammed and Z. Gross, *ACS Catal.*, 2022, **12**, 4310.
57 J. Arnold, *J. Chem. Soc., Chem. Commun.*, 1990, 976.
58 A review: V. W.-W. Yam, V. K.-M. Au and S.-L. Leung, *Chem. Rev.*, 2015, **115**, 7589.
59 Selected articles: (*a*) V. W.-W. Yam, K. M.-C. Wong and N. Zhu, *J. Am. Chem. Soc.*, 2002, **124**, 6506; (*b*) A. Y.-Y. Tam, K. M.-C. Wong and V. W.-W. Yam, *Chem. – Eur. J.*, 2009, **15**, 4775; (*c*) S. Y.-L. Leung, A. Y.-L. Tam, C.-H. Tao, H.-S. Chow and V. W.-W. Yam, *J. Am. Chem. Soc.*, 2012, **134**, 1047; (*d*) K. Zhang, M. C.-L. Yeung, S. Y.-L. Leung and V. W.-W. Yam, *Chem*, 2017, **2**, 825.
60 (*a*) W. Lu, K. T. Chan, S.-X. Wu, Y. Chen and C.-M. Che, *Chem. Sci.*, 2012, **3**, 752; (*b*) V. K.-M. Au, W. H. Lam, W.-T. Wong and V. W.-W. Yam, *Inorg. Chem.*, 2012, **51**, 7537.

61 Selected reports of anionic metal complexes: (*a*) J. R. Berenguer, E. Lalinde and J. Torroba, *Inorg. Chem.*, 2007, **46**, 9919; (*b*) L. Ricciardi, M. L. Deda, A. Ionescu, N. Godbert, I. Aiello and M. Ghedini, *Dalton Trans.*, 2017, **46**, 12625.
62 Y. Tanaka, K. M.-C. Wong and V. W.-W. Yam, *Angew. Chem., Int. Ed.*, 2013, **52**, 14117.
63 Azacalix[3]pyridine derivatives and analogue: (*a*) T. Kanbara, Y. Suzuki and T. Yamamoto, *Eur. J. Org. Chem.*, 2006, 3314; (*b*) N. Uchida, A. Taketoshi, J. Kuwabara, T. Yamamoto, Y. Inoue, Y. Watanabe and T. Kanbara, *Org. Lett.*, 2010, **12**, 5242; (*c*) N. Uchida, J. Kuwabara, A. Taketoshi and T. Kanbara, *J. Org. Chem.*, 2012, **77**, 10631; (*d*) H. Gong, C. Zhang, T. Ogaki, H. Inuzuka, D. Hashizume and D. Miyajima, *Angew. Chem., Int. Ed.*, 2021, **60**, 16377.
64 S. Adachi, M. Shibasaki and N. Kumagai, *Nat. Commun.*, 2019, **10**, 3820.
65 E. Raamat, K. Kaupmees, G. Ovsjannikov, A. Trummal, A. Kütt, J. Saame, I. Koppel, I. Kaljurand, L. Lipping, T. Rodima, V. Pihl, I. A. Koppel and I. Leito, *J. Phys. Org. Chem.*, 2013, **26**, 162.
66 S. A. Smith and W. A. Pretorius, *Water SA*, 2002, **28**, 395.
67 (*a*) H. Maeda, A. Fukui, R. Yamakado and N. Yasuda, *Chem. Commun.*, 2015, **51**, 17572; (*b*) H. Maeda, Y. Takeda, Y. Haketa, Y. Morimoto and N. Yasuda, *Chem. – Eur. J.*, 2018, **24**, 8910; (*c*) N. Fumoto, Y. Haketa, H. Tanaka, N. Yasuda and H. Maeda, *Org. Lett.*, 2021, **23**, 3897; (*d*) M. Yokoyama and H. Maeda, *Chem. Lett.*, 2023, **52**, 598.
68 M. Yokoyama, Y. Okayasu, Y. Kobayashi, H. Tanaka, Y. Haketa and H. Maeda, *Org. Lett.*, 2023, **25**, 3676.
69 S. Sugiura and H. Maeda, *Chem. Commun.*, 2021, **57**, 6983.
70 (*a*) Y. Sasano, N. Yasuda and H. Maeda, *Dalton Trans.*, 2017, **46**, 8924; (*b*) Y. Sasano, Y. Haketa, H. Tanaka, N. Yasuda, I. Hisaki and H. Maeda, *Chem. – Eur. J.*, 2019, **25**, 6712.
71 Selected books and reviews: (*a*) *Supramolecular Chemistry of Anion*, ed. A. Bianchi, K. Bowman-James and E. García-España, Wiley, 1997; (*b*) *Anion Sensing, Topics in Current Chemistry*, ed. I. Stibor, Springer, 2005, vol. 255; (*c*) J. L. Sessler, P. A. Gale and W.-S. Cho, *Anion Receptor Chemistry*, RSC, 2006; (*d*) *Anion Recognition in Supramolecular Chemistry, Topics in Heterocyclic Chemistry*, ed. P. A. Gale and W. Dehaen, Springer, 2010, vol. 24; (*e*) *Anion Coordination Chemistry*, ed. K. Bowman-James, A. Bianchi and E. García-España, Wiley, 2011; (*f*) P. D. Beer and P. A. Gale, *Angew. Chem., Int. Ed.*, 2001, **40**, 486; (*g*) R. M. Duke, E. B. Veale, F. M. Pfeffer, P. E. Krugerc and T. Gunnlaugsson, *Chem. Soc. Rev.*, 2010, **39**, 3936; (*h*) Y. Zhou, J. F. Zhang and J. Yoon, *Chem. Rev.*, 2014, **114**, 5511; (*i*) P. Molina, F. Zapata and A. Caballero, *Chem. Rev.*, 2017, **117**, 9907.
72 Selected original reports: (*a*) H. Maeda and Y. Kusunose, *Chem. – Eur. J.*, 2005, **11**, 5661; (*b*) H. Maeda, Y. Haketa and T. Nakanishi, *J. Am. Chem. Soc.*, 2007, **129**, 13661; (*c*) H. Maeda, M. Terasaki, Y. Haketa, Y. Mihashi and Y. Kusunose, *Org. Biomol. Chem.*, 2008, **6**, 433; (*d*) Y. Haketa and H. Maeda, *Chem. – Eur. J.*, 2011, **17**, 1485; (*e*) Y. Haketa, Y. Bando, K. Takaishi, M. Uchiyama, A. Muranaka, M. Naito, H. Shibaguchi, T. Kawai and H. Maeda, *Angew. Chem., Int. Ed.*, 2012, **51**, 7967; (*f*) R. Yamakado, T. Sakurai, W. Matsuda, S. Seki, N. Yasuda, S. Akine and H. Maeda, *Chem. – Eur. J.*, 2016, **22**, 626; (*g*) A. Kuno, N. Tohnai, N. Yasuda and H. Maeda, *Chem. – Eur. J.*, 2017, **82**, 11166; (*h*) S. Kaname, Y. Haketa, N. Yasuda and H. Maeda, *Org. Lett.*, 2018, **20**, 3268; (*i*) S. Sugiura, W. Matsuda, W. Zhang, S. Seki, N. Yasuda and H. Maeda, *J. Org. Chem.*, 2019, **84**, 8886; (*j*) S. Sugiura, Y. Kobayashi, N. Yasuda and H. Maeda, *Chem. Commun.*, 2019, **55**, 8242; (*k*) S. Sugiura and H. Maeda, *Org. Biomol. Chem.*, 2020, **18**, 4433; (*l*) H. Maeda, T. Nishimura, Y. Haketa, H. Tanaka, M. Fujita and N. Yasuda, *J. Org. Chem.*, 2022, **87**, 7818.
73 Helical structures controlled by ion pairing with chiral counteracation can be applied for the evaluation of conformational changes and optical properties under hydrostatic pressure: T. Kinoshita, Y. Haketa, H. Maeda and G. Fukuhara, *Chem. Sci.*, 2021, **12**, 6691.
74 A review: A. H. Flood, *Beilstein J. Org. Chem.*, 2016, **12**, 611.
75 A review and the first report: (*a*) Y. Hua and A. H. Flood, *Chem. Soc. Rev.*, 2010, **39**, 1262; (*b*) Y. Li and A. H. Flood, *Angew. Chem., Int. Ed.*, 2008, **47**, 2649.
76 (*a*) S. Lee, C.-H. Chen and A. H. Flood, *Nat. Chem.*, 2013, **5**, 704; (*b*) B. Qiao, B. E. Hirsch, S. Lee, S. Lee, M. Pink, C.-H. Chen, B. W. Laursen and A. H. Flood, *J. Am. Chem. Soc.*, 2017, **139**, 6226; (*c*) C. R. Benson, L. Kacenauskaite, K. L. VanDenburgh, W. Zhao, B. Qiao, T. Sadhukhan, M. Pink, J. Chen, S. Borgi, C.-H. Chen, B. J. Davis, Y. C. Simon, K. Raghavachari, B. W. Laursen and A. H. Flood, *Chem*, 2020, **6**, 1978; (*d*) J. Chen, S. M. A. Fateminia, L. Kacenauskaite, N. Bærentsen, S. G. Stenspil, J. Bredehoeft, K. L. Martinez, A. M. Flood and B. W. Laursen, *Angew. Chem., Int. Ed.*, 2021, **60**, 9450; (*e*) J. Chen, S. G. Stenspil, S. Kaziannis, L. Kacenauskaite, N. Lenngren, M. Kloz, A. H. Flood and B. W. Laursen, *ACS Appl. Nano Mater.*, 2022, **5**, 13887; (*f*) L. Kacenauskaite, S. G. Stenspil, A. H. Olsson, A. H. Flood and B. W. Laursen, *J. Am. Chem. Soc.*, 2022, **144**, 19981.
77 H. Tanaka, Y. Haketa, Y. Bando, R. Yamakado, N. Yasuda and H. Maeda, *Chem. – Asian J.*, 2020, **15**, 494.
78 A. Kuno, M. Fujiwara, Y. Haketa and H. Maeda, *Chem. – Asian J.*, 2019, **14**, 1777.
79 N. Koda, Y. Haketa, M. Yokoyama, N. Yasuda and H. Maeda, *Org. Lett.*, 2023, **25**, 1120.
80 A. Kuno, G. Hirata, H. Tanaka, Y. Kobayashi, N. Yasuda and H. Maeda, *Chem. – Eur. J.*, 2021, **27**, 10068.
81 (*a*) E. L. Goff and R. B. LaCount, *J. Am. Chem. Soc.*, 1963, **85**, 1354; (*b*) T. G. Beaumont and K. M. C. Davis, *J. Chem. Soc. B*, 1968, 1010; (*c*) G. Briegleb, J. Trencséni and W. Herre, *Chem. Phys. Lett.*, 1969, **3**, 146; (*d*) M. I. Bruce, P. A. Humphrey, B. W. Skelton and A. H. White, *Aust. J. Chem.*, 1986, **39**, 165; (*e*) G. Maas, H. M. Weber, R. Exner and J. Salbeck, *J. Phys. Org. Chem.*, 1990, **3**, 459.
82 C. Richardson and C. A. Reed, *Chem. Commun.*, 2004, 706.
83 H. Gotoh, S. Nakatsuka, H. Tanaka, N. Yasuda, Y. Haketa, H. Maeda and T. Hatakeyama, *Angew. Chem., Int. Ed.*, 2021, **60**, 12835.

84 A. Takiguchi, H. Tanaka, H. Maeda and H. Shinokubo, *Bull. Chem. Soc. Jpn.*, 2022, **95**, 796.
85 K. Goossens, L. Rakers, B. Heinrich, G. Ahumada, T. Ichikawa, B. Donnio, T. J. Shin, C. W. Bielawski and F. Glorius, *Chem. Mater.*, 2019, **31**, 9593.
86 Reviews: (*a*) R. P. Singh, R. D. Verma, D. T. Meshri and J. M. Shreeve, *Angew. Chem., Int. Ed.*, 2006, **45**, 3584; (*b*) M. Smiglak, A. Metlen and R. D. Rogers, *Acc. Chem. Res.*, 2007, **40**, 1182; (*c*) E. Sebastiao, C. Cook, A. Hu and M. Murugesu, *J. Mater. Chem. A*, 2014, **2**, 8153; (*d*) Q. Zhang and J. M. Shreeve, *Chem. Rev.*, 2014, **114**, 10527; (*e*) M. E. Easton, H. Choudhary and R. D. Rogers, *Chem. – Eur. J.*, 2019, **25**, 2127.
87 Selected reports: (*a*) W. Ogihara, M. Yoshizawa and H. Ohno, *Chem. Lett.*, 2004, **33**, 1022; (*b*) A. R. Katritzky, S. Singh, K. Kirichenko, J. D. Holbrey, M. Smiglak, W. M. Reichert and R. D. Rogers, *Chem. Commun.*, 2005, 868; (*c*) H. Xue, Y. Gao, B. Twamley and J. M. Shreeve, *Inorg. Chem.*, 2005, **44**, 5068; (*d*) C. Ye, J.-C. Xiao, B. Twamley and J. M. Shreeve, *Chem. Commun.*, 2005, 2750; (*e*) M. Smiglak, C. C. Hines, T. B. Wilson, S. Singh, A. S. Vincek, K. Kirichenko, A. R. Katritzky and R. D. Rogers, *Chem. – Eur. J.*, 2010, **16**, 1572; (*f*) G.-H. Tao, M. Tang, L. He, S.-P. Ji, F.-D. Nie and M. Huang, *Eur. J. Inorg. Chem.*, 2012, 3070; (*g*) Q.-H. Lin, Y.-C. Li, Y.-Y. Li, Z. Wang, W. Liu, C. Qi and S.-P. Pang, *J. Mater. Chem.*, 2012, **22**, 666; (*h*) M. Smiglak, C. C. Hines, W. M. Reichert, J. L. Shamshina, P. A. Beasley, P. D. McCrary, S. P. Kelley and R. D. Rogers, *New J. Chem.*, 2013, **37**, 1461; (*i*) L.-L. Dong, L. He, H.-Y. Liu, G.-H. Tao, F.-D. Nie, M. Huang and C.-W. Hu, *Eur. J. Inorg. Chem.*, 2013, 5009; (*j*) C. Yang, L. Chen, W. Wu, C. Zhang, C. Sun, Y. Du and B. Hu, *ACS Appl. Energy Mater.*, 2021, **4**, 146.
88 Ion pairs with tetracyanoallyl anion: (*a*) H. Yasuba, T. Imai and K. Okamoto, *Bull. Chem. Soc. Jpn.*, 1970, **43**, 3101; (*b*) T. Tamamura, M. Yokoyama, S. Kusabayashi and H. Mikawa, *Bull. Chem. Soc. Jpn.*, 1974, **47**, 442; (*c*) T. Tamamura, H. Yasuba, K. Okamoto, T. Imai, S. Kusabayashi and H. Mikawa, *Bull. Chem. Soc. Jpn.*, 1974, **47**, 448; (*d*) T. Tamamura, T. Yamane, N. Yasuoka and N. Kasai, *Bull. Chem. Soc. Jpn.*, 1974, **47**, 832.
89 Ion pairs with hexacyanotrimethylenemethandiide: (*a*) S. Sakanoue, T. Tamamura, S. Kusabayashi, H. Mikawa, N. Kasai, M. Kakudo and H. Kuroda, *Bull. Chem. Soc. Jpn.*, 1969, **42**, 2407; (*b*) S. Sakanoue, N. Yasuoka, N. Kasai and M. Kakudo, *Bull. Chem. Soc. Jpn.*, 1971, **44**, 1.
90 Ion pairs with 1,3-bis(dicyanomethylidene)indan anion: (*a*) E. Saito, T. Yasuhara, Y. Tanaka, R. Yamakado, S. Okada, T. Nohara, A. Masuhara and T. Yoshida, *ECS Trans.*, 2018, **88**, 301; (*b*) Y. Tanaka, K. Ichijo, S. Kodama, S. Aoyama, T. Yoshida, R. Yamakado and S. Okada, *Cryst. Growth Des.*, 2019, **19**, 5811.
91 C. Reichardt, *Chem. Rev.*, 1994, **94**, 2319.
92 P.-A. Bouit, D. Rauh, S. Neugebauer, J. L. Delgado, E. D. Piazza, S. Rigaut, O. Maury, C. Andraud, V. Dyakonov and N. Martin, *Org. Lett.*, 2009, **11**, 4806.
93 I. Baraldi, F. Momicchioli, G. Ponterini, A. S. Tatikolov and D. Vanossi, *J. Phys. Chem. A*, 2001, **105**, 4600.
94 Z. Li, S. Mukhopadhyay, S.-H. Jang, J.-L. Brédas and A. K.-Y. Jen, *J. Am. Chem. Soc.*, 2015, **137**, 11920.
95 S. Kusabayashi, A. Taniguchi and H. Mikawa, *Bull. Chem. Soc. Jpn.*, 1966, **39**, 1344.
96 (*a*) E. D. Owen and Q. Sultana, *J. Appl. Chem. Biotechnol.*, 1972, **22**, 1043; (*b*) I. Willner, Y. Eichen, A. Doron and S. Marx, *Isr. J. Chem.*, 1992, **32**, 53; (*c*) I. Willner, Y. Eichen, M. Rabinovitz, R. Hoffman and S. Cohen, *J. Am. Chem. Soc.*, 1992, **114**, 637.
97 N. C. Yang and A. J. Castro, *J. Am. Chem. Soc.*, 1960, **82**, 6208.
98 S. Sugiura, T. Kubo, Y. Haketa, Y. Hori, Y. Shigeta, H. Sakai, T. Hasobe and H. Maeda, *J. Am. Chem. Soc.*, 2023, **145**, 8122.
99 The space group of the single crystal of **22d**$^{+}$-**38a**$^{-}$ is triclinic *P*1, which induces polarization caused by inhomogeneous stacking.
100 A review on supramolecular ferroelectrics: A. S. Tayi, A. Kaeser, M. Matsumoto, T. Aida and S. I. Stupp, *Nat. Chem.*, 2015, **7**, 281.
101 S. Takizawa, T. Okuyama, S. Yamazaki, K. Sato, H. Masai, T. Iwai, S. Murata and J. Terao, *J. Am. Chem. Soc.*, 2023, **145**, 15049.
102 Very recent examples: R. Sengupta, H. Hashimoto, Y. Haketa, H. Sakai, T. Hasobe and H. Maeda, *Org. Lett.*, 2023, **25**, 6040.

